# ANALYSIS OF GLASS, CERAMIC, AND SOIL SAMPLES USING LASER ABLATION INDUCTIVELY COUPLED PLASMA MASS SPECTROMETRY

By

SCOTT A. BAKER

A DISSERTATION PRESENTED TO THE GRADUATE SCHOOL
OF THE UNIVERSITY OF FLORIDA IN PARTIAL FULFILLMENT
OF THE REQUIREMENTS FOR THE DEGREE OF
DOCTOR OF PHILOSOPHY

UNIVERSITY OF FLORIDA

1998

ACKNOWLEDGMENTS

I would like to thank my research advisor, Dr. James D. Winefordner, for his patience, guidance, encouragement, and enthusiasm. I consider myself extremely fortunate to have had the opportunity to work under his direction. I would also like to thank Dr. Benjamin W. Smith for many useful discussions concerning this research and for always having an open door. Both of these people were integral in my development as a scientist.

I am grateful to all of the members of the Winefordner research group for their friendship. They were a source of inspiration and helped me a great deal in producing this work. I would especially like to acknowledge those who contributed directly to my experiments. These people included Igor Gornushkin, David Rusak, Bryan Castle, Robin Russell, Melody Bi, Rebecca Litteral, Matthew Dellavecchia, and Ricardo Aucelio. Additionally, I would like to acknowledge Dr. Kobus Visser, Dr. Oleg Matveev, and Dr. Nico Omenetto for many useful discussions during the course of my graduate studies.

I thank Jeanne Karably for answering many questions and for making sure things went smoothly. Also, I would like to acknowledge Steve Miles for his electronics expertise, and Joe Shalosky, Gary Harding, and Dailey Burch of the machine shop for helping me on many occasions.

I am grateful to Dr. Paul Holloway and Dr. Steve Pearton for use of their profilometers, and to the staff at the Major Analytical Instrumentation Center for

allowing me to use their facilities. They also produced the electron microprobe data.

My parents have always provided me with love and support. They have been a great source of strength and encouragement throughout my life. I cannot express enough how much the love, support, and friendship of my wife, Amy, means to me each and every day. She has always been there to keep me going, and to keep things in perspective. I look forward to our spending a long and joyous life together.

Finally, I would like to acknowledge the National Science Foundation-Engineering Research Center for Particle Science and Technology and the Air Force Office of Scientific Research for funding this research.

TABLE OF CONTENTS

ACKNOWLEDGEMENTS....ii

ABSTRACT....vii

CHAPTERS

1 INTRODUCTION....1

2 BACKGROUND....6

Inductively Coupled Plasmas....6
Inductively Coupled Plasma-Mass Spectrometer Interface....10
Ion Optics....12
Mass Analyzer....13
Detection of Ions....14
Sample Introduction in ICP-MS....14
Laser Ablation....16

3 GENERAL CONSIDERATIONS AND OPTIMIZATION OF EXPERIMENTAL PARAMETERS....19

Introduction....19
Instrumentation....19
Samples....21
Results....22
Plasma Operating Conditions....22
Scan Parameters and Internal Standardization....33
Sampling Strategy....35

4 ANALYSIS OF GLASS SAMPLES....41

Introduction....41
Experimental....42
Calibration Procedure....43
Results....47
Fractionation....47
Solution-Based Calibration....53

Spot Sampling Versus Line Sampling....58
Conclusions....69

5 ANALYSIS OF SILICON NITRIDE CERAMIC BEARINGS....70

Introduction....70
Experimental....72
Results....73
Identification and Distribution of Elements in Silicon Nitride....73
Results from Solution- and Glass-Based Calibration....78
Measurement of Mass Ablated and
Estimation of System Efficiency....82
Conclusions....84

6 INVESTIGATION OF LIGHT SCATTERING
FOR MASS NORMALIZATION IN LA-ICP-MS....85

Introduction....85
Experimental....86
Results....90
Scatter Signal Normalization and Comparison
with Internal Standardization....90
Comparison of Scatter Normalization for Glass,
Soil, and Macor® Ceramic....96
Conclusions....103

7 ANALYSIS OF SOIL AND SEDIMENT SAMPLES....104

Introduction....104
Experimental....105
Results....108
Spot Sampling Versus Line Sampling....108
Solution-Based Calibration....110
Speciation Effects....117
Effect of Organic Content....121
Analysis of Particle Size Fractions....125
Analysis of Soils Using Standard Additions....130
Detection Limits....134
Conclusions....134

8 EVALUATION OF A COMPACT LASER SOURCE....136

Introduction....136
Experimental....137
Results....138
Conclusions....146

9 CONCLUSIONS AND FUTURE WORK....147

Conclusions....147
Future Work....150

REFERENCES....153

BIOGRAPHICAL SKETCH....159

Abstract of Dissertation Presented to the Graduate School
of the University of Florida in Partial Fulfillment of the
Requirements for the Degree of Doctor of Philosophy

# ANALYSIS OF GLASS, CERAMIC, AND SOIL SAMPLES USING LASER ABLATION INDUCTIVELY COUPLED MASS SPECTROMETRY

By

Scott A. Baker

May 1998

Chairman: James D. Winefordner
Major Department: Chemistry

Laser ablation (LA) as a direct solid sampling method for inductively coupled plasma mass spectrometry (ICP-MS) has been used for the analysis of glass, ceramic, and soil samples. The strength of this technique is that it can be applied to essentially any solid material and eliminates the need for difficult and time consuming dissolution procedures. The major limitation of LA-ICP-MS is the presence of matrix effects, making quantitation difficult in the absence of standards of identical composition.

This work was largely concerned with the development of methodology for obtaining accurate quantitative results from a variety of solid materials, including glasses, ceramics, and soils without the need for matrix-matched standards. The use of solution-based calibration for the analysis of a National Institute of Standards and Technology (NIST) glass resulted in excellent agreement (typically +/- 10%) with the certified values. Detection limits were in the sub-ppm range for all elements studied. The solution

calibration technique was also applied to silicon nitride ceramic bearings and the accuracy of the results were confirmed with X-ray microanalysis. In addition, standard glass materials were useful in the analysis of ceramics provided that differences in ablated mass were properly accounted for. To this end, the use of light scattering for measuring the amount of ablated material was evaluated. Light scattering was effective for mass normalization provided that the particle sizes of the ablation products were sufficiently similar.

The use of solution-based calibration for soil samples resulted in poorer agreement than in the case of glasses and ceramics; however, results were still within +/- 20 % for most analytes studied. Studies involving sample particle size, organic content, and element speciation were performed to understand the effects that these variables have on LA-ICP-MS measurements. The use of standard additions was briefly studied. It was concluded that this technique is useful, provided the particle sizes in the sample are sufficiently small.

A compact, inexpensive laser was also evaluated for LA-ICP-MS measurements. It was used for the analysis of glass and aluminum samples and provided low to sub-ppm detection limits for the analytes studied.

# CHAPTER 1
# INTRODUCTION

Developments in materials research, environmental science, industrial quality control protocols, and numerous other endeavors have placed a high premium on the development of accurate and sensitive analytical techniques. The presence of trace element impurities in ceramics, for example, have been shown to affect the physical and mechanical properties of these materials (1). In the electronics industry, the presence of alkali and alkaline earth metals may cause corrosion and degradation of microelectronic devices. In addition, the alpha emitters U and Th can cause errors in storage devices (2). Therefore, the presence of these elements and their concentrations must be accurately determined. Geologists need to determine absolute and relative concentrations of elements in a variety of geological samples, in an effort to discover the principles governing their distribution and migration (3). In addition, the ability to precisely measure isotopic ratios of such elements as Li, Sr, Nd, Pb, and U is important for the radiogenic dating of materials and providing an understanding of terrestrial processes (3, 4). The effects of heavy metals (e.g. Pb, Cr, Hg, and Cd) on human health are well established and techniques for monitoring suspected areas of contamination, such as soils, are required (5, 6). Furthermore, research has shown that the presence of particular elements (e.g. Se) results in some protection against heavy metal toxic effects; therefore, it is important to be able to monitor the presence of several elements in the sample of

interest (7). It is evident that precise and accurate measurement of multiple elements at low levels is required in a variety of applications.

In many cases the sample of interest is a solid and the ability to analyze the material directly would be beneficial. Direct analysis of solids eliminates the need for the time-consuming digestion and dissolution procedures required for many materials. In addition, there is a reduced risk of sample contamination, incomplete digestion, or the loss of some analytes during sample preparation. Lower absolute detection limits are also possible since there is no dilution of the sample prior to analysis. In some instances, the local concentration of analytes is of greater importance than the bulk concentration and this information is completely lost with dissolution of the original sample. In these cases, the ability to probe particular areas of the solid is essential and techniques capable of microanalysis are needed.

Several of the techniques commonly used for the elemental analysis of solids are X-ray fluorescence (XRF) (8), electron probe microanalysis (EPMA) (9), secondary ion mass spectrometry (SIMS) (10), and glow discharge mass spectrometry (GDMS) (11). Each of these techniques has its strengths and weaknesses. XRF is a well established technique for the analysis of conducting and nonconducting solids; however, it suffers from relatively poor detection limits (10-100 ppm) and significant matrix effects when analyzing thick samples (3, 8). In addition, it is essentially a bulk technique and provides poor spatial resolution. EPMA is a valuable surface analysis technique due to the high spatial resolution (0.1-0.5 μm) that it provides. The technique is limited by high relative detection limits (100-1000 ppm), sample charging with nonconducting samples, and the requirement that the sample be held in vacuum. In addition, quantitative work requires a

highly polished surface and strict matrix-matching (9). SIMS is another technique for surface analysis, but unlike EPMA, it offers very high sensitivity with detection limits as low as 1 ppb (10). It is widely used for depth profiling studies because of its high in-depth resolution (1-2 nm). Lateral resolution is typically around 0.1-1 μm (10). Like EPMA, sample charging is a major problem when analyzing nonconducting samples and the sample must be held in vacuum. In addition, matrix effects are very severe making quantitation extremely difficult (12, 13).

GDMS is a technique which has been widely used for the analysis of conducting samples. This is due to low detection limits (1-100 ppb) and high measurement precision (11). Nonconducting samples can be analyzed by diluting the sample in a conductive matrix (11), using a secondary cathode (14), or by operating the glow discharge in the rf mode (15). The latter technique has shown considerable promise for the analysis of nonconductors (e.g. ceramics and glasses), but a major challenge to accurate quantitative measurements is matrix effects based on sample thickness. The GD technique can be used for depth profiling studies with a resolution approaching 100 nm. The lateral resolution; however, is usually only a few millimeters (16). A major benefit associated with GDMS, like SIMS, is that it provides isotopic information by virtue of its detection methodology.

The use of laser ablation inductively coupled plasma mass spectrometry (LA-ICP-MS) for the analysis of solid samples compares favorably with other techniques. A focused, pulsed laser beam can be used to sample essentially any type of material and when combined with the high sensitivity of ICP-MS, the technique offers sub-ppm detection limits for most elements. Because the sampling and excitation steps are

separate, each can be independently controlled for optimum performance. This results in reduced matrix effects compared to single step laser based techniques, such as laser microprobe mass analysis (LAMMA) (17). Laser sampling also allows for modest spatial profiling of the sample with lateral resolutions on the order of microns and in-depth resolution on the sub-micron scale. Mass spectrometric detection also allows for the measurement of isotopic ratios. The versatility of the technique is evidenced by the many types of samples which have been analyzed, including metals, glasses, ceramics, geological materials, biological materials, and polymers. One major advantage of LA-ICP-MS compared to other solids techniques is that the sample can generally be analyzed without any modification and is held at atmospheric pressure. This results in rapid sample changing and increased throughput. In addition, elemental sensitivity factors for LA-ICP-MS are relatively uniform for most elements when compared with many other solids techniques. This makes the technique excellent for semiquantitative analyses (12); however, quantitative measurements by LA-ICP-MS are often difficult to obtain.

The major difficulty associated with laser sampling is the complex nature of laser-material interactions (18). This results in an unknown quantity of material being ablated with a composition which may or may not accurately reflect the bulk sample. The properties of the ablated material (e.g. composition and particle size distribution), depend on the laser and material characteristics. Because of the complex nature of the laser sampling process, matrix-match standards are often required for quantitative measurements on a given sample. This represents the major obstacle to the widespread applicability of the technique, since for many solid matrices, suitable standards are not readily available. To overcome these difficulties, approaches such as the use of fused

glass beads (19, 20) or pelletized mixtures of diluent and analyte (20, 21) have been explored. Although useful in some cases, the sample preparation that is required eliminates a major advantage associated with laser sampling and any spatial variations cannot be assessed.

The intent of the present work is to develop methodology for the accurate and precise determination of analytes in a variety of solid matrices, including glass, silicon nitride ceramic, and soil, by LA-ICP-MS. Optimum experimental parameters were determined and the effectiveness of solution-based calibration for the analysis of solids was evaluated. In addition, the utility of glass standard reference materials for calibration of ceramics was examined. As an alternative to internal standardization, mass normalization by measuring light scattering from the ablated material was studied. Its applicability for various sample types was assessed. A compact, inexpensive laser source was evaluated for the analysis of glass, copper, and aluminum samples. Future research directions are suggested based on these studies.

# CHAPTER 2
# BACKGROUND

The inductively coupled plasma (ICP) has developed into the dominant excitation source for elemental analysis. Its initial development was as an excitation source for atomic emission spectroscopy (AES); however, in the past decade it has been widely used as an ion source for mass spectrometry. Numerous publications dealing with the fundamentals of inductively coupled plasma-mass spectrometry (ICP-MS) and some applications are available (22-27). The major benefits of ICP-MS, compared to ICP-AES, are superior detection limits, spectral simplicity, and the ability to measure isotope ratios. Detection limits for solutions are typically 100-1000 times better for ICP-MS, with typical values for most elements in the 1-100 ppt range. Mass spectra of the elements are simple and unique. The natural isotopic abundance spectral pattern provides a simple means of identifying sample constituents. The ability to measure isotopic ratios is important in geological and nuclear applications; however, it also allows one to assess the existence and extent of interferences. The major components of a typical ICP-MS are the ICP, an interface system, ion lenses, mass analyzer, and a detector. These will be discussed in greater detail.

## Inductively Coupled Plasmas

The ICP is a partially ionized gas maintained by energy coupled to it from a radio frequency (RF) generator, typically operated at 27 or 40 MHz. Energy, usually between 1 and 2 kW, is coupled to the plasma with a 2-4 turn copper coil which acts as the

primary of an RF transformer. The plasma itself acts as the secondary. Argon (Ar) is typically used as the plasma gas, although hydrogen-argon, nitrogen-argon, xenon-argon, and helium plasmas have been studied as well (22). The plasma is generated inside and at the end of a quartz torch, which consists of an assembly of quartz tubes. An illustration of the ICP torch is given in Figure 2-1. The outer gas flow (coolant) is typically 10-15 L $min^{-1}$ and serves both to protect the tube walls from melting and as the main plasma support gas. The middle annular flow (auxiliary or intermediate) is used to keep the plasma from melting the central injector tube. Typical values for this flow are 0.5-1.0 L $min^{-1}$. The inner gas flow (nebulizer or carrier) is used to puncture the plasma and inject aerosol from the sample introduction system. This flow is typically in the range of 0.7-1.0 L $min^{-1}$.

The copper load coil is positioned around the end of the torch and supplied with RF current. This produces a time varying magnetic field (27 or 40 MHz) which lies along the torch axis. A Tesla coil is used to seed the Ar flow with free electrons. These electrons precess around the magnetic field in circular orbits and the energy supplied to the coil is converted into kinetic energy of the electrons. At atmospheric pressure, the free electron path before colliding with Ar atoms is only around $10^{-3}$ mm; therefore, the plasma is rapidly heated and a bright discharge is formed (23).

At the RF frequencies used, the skin effect is occurring which ensures that most of the energy is coupled to the induction region of the plasma. The nebulizer gas punches a channel through the center of the plasma and there is little mixing with the outer annular region. Heat is transferred to this central gas flow mainly by radiation and conduction from the annular induction region. Gas kinetic temperatures in the central

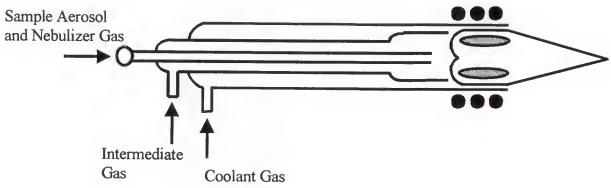


Figure 2-1. Inductively coupled plasma torch.

region are typically between 5000-7000 K, while the temperature in the outer region is as high as 10,000 K (23). It is important that the power is coupled mainly into the outer region where there is little interaction with the sample aerosol. This is because the sample composition can vary significantly and have only minimal effects on the plasma sustaining processes. Separation of the energy coupling and sample excitation region is one of the major reasons why the ICP is characterized by relatively few chemical and physical interferences.

The role of the plasma is to convert the sample into free ions. Most analyte ion formation results from collisions of electrons, and the probability of this process is dependent on the electron density ($\sim 10^{15}$ $cm^{-3}$) and temperature (26). The gas temperature, which describes the kinetic energy of Ar atoms, controls the desolvation and vaporization of the sample aerosol. Transit times through the center of the plasma are typically several milliseconds; therefore, desolvation, vaporization, atomization, and ionization processes occur very efficiently. The degree of ionization is dependent on the ionization conditions in the plasma, which are dominated by the major plasma constituent (typically Ar, H, O, and electrons) and the partition function and ionization energy for the atom of interest (23). The Saha equation, though not strictly valid since thermal equilibrium does not exist in the plasma, is often used to give insight into ionization conditions in the plasma. Under normal operating conditions, elements with ionization energies of 8 eV or less (approximately half of the elements in the periodic table) are >90 % ionized in the plasma, while Ar with an ionization energy of 15.75 eV is only about 1% ionized (27). In addition, only a few elements (e.g. Ba, Sr, and Pr) have second

ionization energies low enough to produce a significant population of doubly charged ions. The end result is a very efficient ion source for primarily singly charged ions.

Inductively Coupled Plasma-Mass Spectrometer Interface

The ability to extract ions representatively from the plasma is obviously quite critical in ICP-MS. A description of the ICP-MS interface is provided with particular emphasis on the interface used in this work (Figure 2-2). It consists of three cones through which the pressure drops from atmosphere to approximately $10^{-5}$ torr by means of differential pumping. The first cone, the sample cone, is located approximately 13 mm from the top of the load coil and has an orifice of 1.1 mm. The region behind the sample cone is maintained at 2-3 torr by a mechanical pump. This results in the formation of a supersonic jet expansion. The jet consists of a freely expanding region, the zone of silence, surrounded by shock waves called the barrel shock and Mach disc. Shock waves result from collisions between the supersonic jet and residual gas in the expansion chamber. To avoid losses of ions due to collisions and scattering, the second cone (skimmer) is positioned before the Mach disc inside the zone of silence. Studies have indicated that maximum ion transmission occurs when the sampler-skimmer distance is approximately 2/3 of the distance to the onset of the Mach disc (28). The location of the skimmer cone is 8 mm from the sample cone and the diameter orifice is 0.8 mm to allow the centerline of the expansion to pass while removing the cooler gas at the edge of the supersonic jet (29). Only about 1% of the gas that is sampled passes through the skimmer cone. The pressure in the region behind the skimmer cone is maintained at $10^{-3}$ torr by a turbomolecular pump.

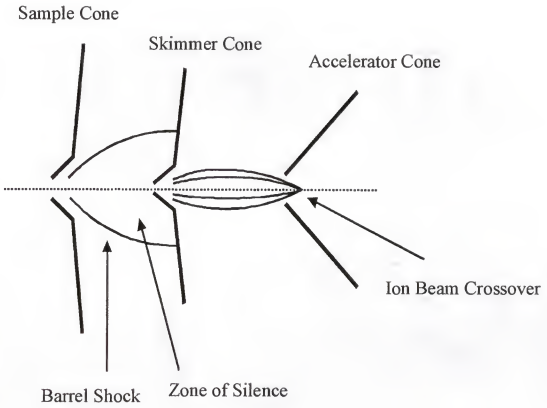


Figure 2-2. Schematic of ICP-MS interface.

Unique to the Finnigan MAT SOLA used in this work is the incorporation of an accelerator cone. It is located 10 mm behind the skimmer cone and has a +2 kV potential applied to it. The lens is used to focus the ions that pass through it and accelerate them to the ion optics. The purpose for this will be presented more clearly in the discussion on ion optics.

## Ion Optics

The purpose of the ion optics is to supply the quadrupole with ions of low enough energy that they can be efficiently differentiated with respect to their mass to charge ratios. Ions must be separated from neutrals, and photons produced from the plasma must be removed since these can activate the detector and contribute significantly to the background. Typically, a Bessel box has been employed for separating these components. The Bessel Box consists of a central photon stop for removing photons, while neutrals are removed by pumping of the chamber. Ions are electrostatically steered around the photon stop and refocused into an exit slit. This arrangement results in two detrimental effects; space charge effects and mass dependent focusing of the ion beam (29). Space charge effects are more significant for lighter ions since they are more easily deflected from their flight path. Mass dependent focusing results because different mass ions have different kinetic energies and thus have different paths through the ion lenses. Therefore, optimization of ion transmission is mass dependent and a compromise setting must be used. This is typically in the mid mass range for multielement work, resulting in a transmission profile which falls off at the low and high mass ends. The Finnigan MAT

SOLA ICP-MS accelerator cone and ion optics are designed to reduce these effects and produce a more even transmission profile.

The accelerator cone supplies a high velocity stream of ions condensed in a tightly focused beam. This beam is deflected off axis and realigned to exit parallel to the original ion transmission, since ion losses of 50-80% have been measured when photon stops are used (23). In addition, because the residence time in the ion optics is shorter with the accelerated beam, space charge effects will be less significant. Since the beam has not been defocused and refocused, as is the case with the Bessel Box, no mass dependent transmission effects have been introduced. The final stage of the ion optics is a phase matching lens that reduces ion velocities to the level required by the quadrupole.

## Mass Analyzer

Several types of mass analyzers have been employed for ICP-MS, including quadrupoles, magnetic sectors (30), time of flight (31), and ion traps (32). Only a discussion of quadrupoles is provided here, since it was used in this work.

The quadrupole consists of four straight metal rods arranged parallel to and equidistant to the ion axis. Opposite rods are connected together with DC and RF voltages applied to each pair. The DC voltage is positive for one pair and negative for the other. The RF voltages on each pair are 180° out of phase. Appropriate amplitudes of these potentials produce trajectories for ions along the quadrupole which are stable for only one particular mass to charge ratio. By keeping these potentials constant, single ion monitoring is accomplished. To produce a mass scan, the amplitudes are varied while keeping the RF to DC ratio constant. The mass transmitted is linearly related to the

magnitude of the RF and DC voltages. Peak jumping between masses of interest is accomplished by rapidly selecting discrete values of RF and DC voltages. The use of rapid and repetitive peak jumping is extremely important when dealing with transient or highly fluctuating signals, such as those typical of LA-ICP-MS. The mass resolution is determined by the ratio of RF and DC voltages. This is typically set to provide 1 amu peaks across the mass range (5-240 amu).

## Detection of Ions

Detection of ions is most often accomplished with a channeltron electron multiplier. This detector is characterized by high gain ($\sim 10^8$), low dark current, and fast response time. Output pulses from the detector are sensed by a fast pre-amplifier and sent to a discriminator and counting circuit. The detector is used for signal rates between 1 and $10^6$ counts/second. For higher ion currents, a Faraday collector plate is used. This detector can be used for ion signal rates between $\sim 10^5$ and $5 \times 10^{10}$ counts/second; however, the time constant of the DC amplifier limits the Faraday to relatively low scan rates (64 ms or greater). In the Finnigan MAT SOLA, selection of the detector is accomplished electronically by deflection of the ion beam to the appropriate detector.

## Sample Introduction in ICP-MS

Samples are introduced to the ICP-MS as gas, vapor or a fine aerosol of solution, or as solid particles. Pneumatic nebulization of solutions is the most common means of sample introduction, due to its simplicity, sufficient stability, and an overall greater understanding of the process. Although this dissertation is concerned with the

introduction of solid particles by laser ablation, mention is made of solution introduction since it was often used in this work.

The principle behind pneumatic nebulizers is the disruption of a liquid stream by a high velocity gas, resulting in the production of aerosol droplets. The liquid stream is provided by a peristaltic pump which typically produces a 1 mL $min^{-1}$ flow. In the concentric type of nebulizer used in this work, liquid is introduced to a fine central capillary and when the liquid reaches the tip, it is broken into fine droplets by the shearing action of Ar gas flowing around the orifice at 0.5-1.0 L $min^{-1}$. The liquid particles produced can be as large as 100 μm; therefore, they must be further processed before entering the ICP-MS. This is accomplished with a Scott-type double pass spray chamber, which acts as a low pass filter. Larger particles settle out and only particles <10 μm are transported to the plasma.

The introduction of solutions, typically aqueous with small amounts of acid, results in a large number of spectroscopic interferences. The dissociation of water produces large amounts of oxygen and thus the presence of oxide species can be significant. In addition, the constituents of acids used will also contribute to the background spectrum. For this reason, nitric acid is often the preferred acid since its constituents (H, N, and O) are already present in the plasma (23). Numerous methods have been employed to decrease the solvent plasma load, such as cooled spray chambers (33), Peltier effect coolers (34), membrane interfaces (35), and heater condensers (36).

Several techniques have been employed for introducing solids into the ICP-MS. The uses and relative merits of these techniques are discussed in several reviews (22, 23,

27). They include slurry nebulization, electrothermal vaporization (ETV), direct sample insertion (DSI), arc and spark ablation, and laser ablation (LA). Of these techniques, the last (LA) is most promising since it can be used to sample a wide range of materials. In addition to bulk analyses, it also allows for microanalysis by virtue of the focusing characteristics of lasers. These attributes put laser ablation in a unique position among solid sampling techniques for ICP-MS. The first application of LA-ICP-MS was reported by Alan Gray in 1985 (37). Since that time, the technique has been used to analyze a wide variety of materials, including metals (38, 39), glasses (19, 20, 40), ceramics (41, 42), geological materials (43, 44), biological materials (45), and polymers (46).

## Laser Ablation

The ablation process (Figure 2-3) depends on a large number of factors, including the nature of the solid material, laser characteristics (wavelength, pulse duration, etc.), and pressure and composition of the gas medium. Nonetheless, a phenomenological description can be given. When a short duration pulse of sufficient energy (typically irradiances $> 10^8$ W cm $^{-2}$) strikes the sample, the surface is instantaneously heated past its vaporization temperature through linear one-photon absorption, multi-photon absorption, dielectric breakdown, and additional undefined mechanisms (47, 48). Energy dissipation of the surface layer is slow relative to the laser pulse duration and before this layer can vaporize underlying layers have reached their vaporization temperature. The underlying layers reach the critical point (temperature and pressure) resulting in an explosion of the surface. This process is described as nonthermal and so no fractional vaporization should occur (18). During the ablation process, a plasma is initiated on the surface with temperatures in the range of $10^4$-$10^5$ K (47, 48) and a duration of several

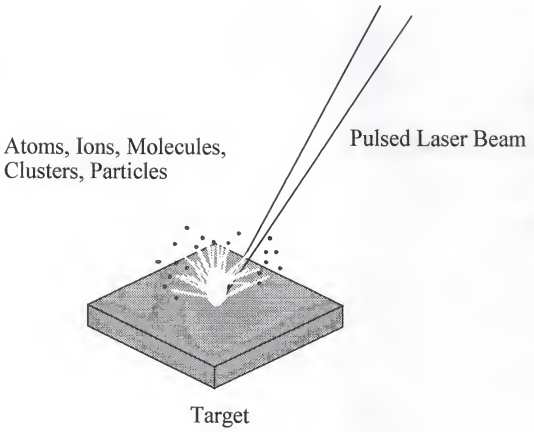


Figure 2-3. Conceptual drawing of laser ablation.

microseconds. This also interacts with the sample surface and contributes to the quantity and composition of the ablated material.

In addition to LA-ICP-MS, numerous other uses of laser ablation have been explored. An excellent review by Darke and Tyson deals with fundamental aspects of laser ablation and its uses in analytical spectrometry (17). These include techniques which directly use the laser induced plasma as an excitation source (laser induced breakdown spectroscopy - LIBS) (49), ionization source (laser microprobe mass spectroscopy - LAMMA) (50), or atom reservoir (laser ablation laser excited atomic fluorescence spectroscopy - LA-LEAFS) (51). As in LA-ICP-MS, laser ablation has been used as a method of sample introduction for numerous analytical techniques including flame and furnace atomic absorption (52, 53), glow discharge atomic emission (54), and microwave induced plasma atomic emission (55). The major advantage of separating the laser sampling step from spectroscopic detection is that it allows for independent optimization of each step, potentially resulting in improved analytical performance.

# CHAPTER 3
# GENERAL CONSIDERATIONS AND OPTIMIZATION OF EXPERIMENTAL PARAMETERS

## Introduction

The purpose of this chapter is to outline several of the key variables that affect LA-ICP-MS measurements. It is intended to serve as a guide in the selection of appropriate experimental conditions. The measurements have been performed on a variety of samples (metals, glasses, ceramics, and soils); however, the goal is to provide information that is generally applicable to all matrices. More specific information on particular materials can be found in subsequent chapters.

## Instrumentation

An illustration of the LA-ICP-MS setup is shown in Figure 3-1. It consists of a Finnigan MAT SOLA ICP-MS (Hemel Hempstead, UK) and System 266 laser ablation accessory. The ablation module consists of a Spectron SL 401 Nd:YAG laser which has been frequency quadrupled to produce an output beam of 266 nm, as well as beam steering and focusing optics and a CCD camera for remote viewing of the sample. The CCD camera is mounted in parallel with the laser and aids in focusing of the laser beam. The system also includes an x-y-z translation stage for adjusting the focus of the laser beam and for selecting the area of the sample for analysis. The system is designed to provide analysis only at a fixed location. However, it was modified to allow for translation of the sample while the laser was firing. Laser repetition rates of up to 5 Hz

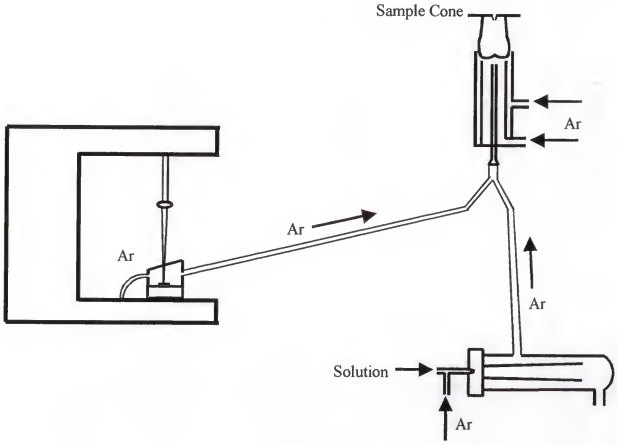


Figure 3-1. LA-ICP-MS System

can be utilized, with pulse energies of ~ 0.1-1 mJ and pulse widths around 15 ns in duration. When focused to a 50 μm spot, laser irradiances ($W/cm^2$) of ~ $8x10^7$-$8x10^8$ are achieved.

For analyses, the sample is placed in an ablation cell consisting of a 6 cm glass tube with a quartz window for transmission of the UV laser beam. The cell has a total volume of ~ 100 $cm^3$. Ablated material is swept out of the ablation cell and to the ICP-MS through 1.5 m of 3/16" i.d. plastic tubing with a flow of argon. In addition, the output from a concentric nebulizer and cooled Scott-type spray chamber can also be continuously introduced to the ICP-MS during ablation with a glass Y-connector. This dual sample introduction approach is termed "wet plasma" operation (38). A comparison of wet and dry (ablation chamber flow only) plasmas will be made later in this chapter. The ICP is typically operated between 1100 and 1300 W with coolant and intermediate flows of 15 L/min and 0.9 L/min, respectively. Sample is carried to the plasma, whether from the ablation chamber, nebulizer, or a combination of both, with a total argon flow of ~1 L/min.

## Samples

Various samples were used in these studies. They included National Institute of Standards and Technology (NIST) (Gaithersburg, MD) glasses, silicon nitride ceramic bearings, various metals, and NIST soil samples. The soil samples were pressed into 1 cm pellets at a pressure of 5 MPa. No binder was required to produce relatively rigid pellets. The only constraints on sample size were that they fit into the ablation chamber and the height match the range of the stepper motor used to adjust the focusing lens position. This stepper motor could be adjusted over a range of 1.25 cm and the lower

focusing position corresponded to a point ~0.2 cm above the base of the ablation cell. Therefore, samples with thicknesses ranging from 0.2 cm to 1.45 cm could be analyzed without any modification.

## Results

Several experimental variables were investigated. These include plasma operating conditions (wet and dry plasmas, RF power, and argon flow rate), laser sampling mode (stationary or translated sample), and detection considerations (scan parameters and internal standardization).

### Plasma Operating Conditions

Among the attributes often cited for laser ablation as a sample introduction technique is the elimination of solvents and hence, the resulting diminished level of many background peaks. A comparison of background spectra from wet and dry plasmas illustrated this point (Table 3-1). The dry plasma was operated at 950 W with a 1.0 L/min flow from the ablation chamber, while the wet plasma was operated at 1300 W with a nebulizer flow rate of 0.65 L/min and an additional 0.35 L/min from the ablation chamber. These operating conditions were chosen because they provided the highest analyte signals for laser ablation measurements. In the wet plasma mode, a 2 % $HNO_3$ solution was introduced to the nebulizer at 1 mL/min with a peristaltic pump (Gilson Minipulse 3, Middleton, WI). Table 3-1 lists some of the major background peaks. In each case, the background level is significantly larger for the wet plasma. In addition, the introduction of solution can introduce trace levels of impurities even for high purity reagents. The peak at m/z 58 was partially due to the Ni sampling cone.

Table 3-1. Comparison of wet and dry plasma background.

| Background Species (m/z) | Dry Plasma Signal (counts/s) | Wet Plasma Signal (counts/s) |
|---|---|---|
| $CO^+$, $N_2^+$ (28) | $3.3x10^5$ | $1.0x10^7$ |
| $N_2H^+$ (29) | $1.9x10^5$ | $1.3x10^6$ |
| $NO^+$ (30) | $3.8x10^6$ | $3.0x10^8$ |
| $ArH_2^+$ (42) | $3.2x10^4$ | $2.4x10^6$ |
| $ArN^+$ (54) | $2.5x10^5$ | $1.5x10^7$ |
| $ArO^+$ (56) | $1.3x10^5$ | $6.5x10^6$ |
| $ArO^+$, $Ni^+$ (58) | 2300 | 6200 |

The effect of RF power on analyte signal for both dry (a) and wet (b) plasmas is shown in Figure 3-2. The $^{63}Cu$ signal was measured from laser ablated brass samples as a function of RF power. As previously indicated, the wet plasma optimizes at higher RF powers for the same total flow (1.0 L/min) through the torch injector tube. The reason for this behavior was the energy required in vaporizing the solution aerosol. It should also be mentioned that RF power optimization only applied to particular flow conditions, since these variables were interactive. For example, if the flow was kept at 1 L/min and the ratio of nebulizer gas to ablation chamber gas was increased, a higher RF power was required for maximum analyte signals due to the increased solvent loading. For both wet and dry plasmas, increasing the total flow through the injector tube required higher RF powers for efficient ionization.

Optimized plasma conditions were more easily determined for the dry plasma since only two variables (RF power and argon flow) were involved. The RF power was adjustable over the range of 950-1450 W for stable plasma operation. With the wet plasma, the nebulizer flow rate was more difficult to optimize. To gain insight into the proper nebulizer and ablation chamber flow rates, the RF power was held constant at 1350 W while the nebulizer and ablation chamber flow rates were systematically varied. Total argon flow rates between 0.8 and 1.2 L/min with individual flows from 0.2 and 1.0 L/min were studied. These studies indicated that ablation chamber flows of 0.3-0.4 L/min and nebulizer flows of 0.6-0.7 L/min were most suitable in terms of both sensitivity and precision.

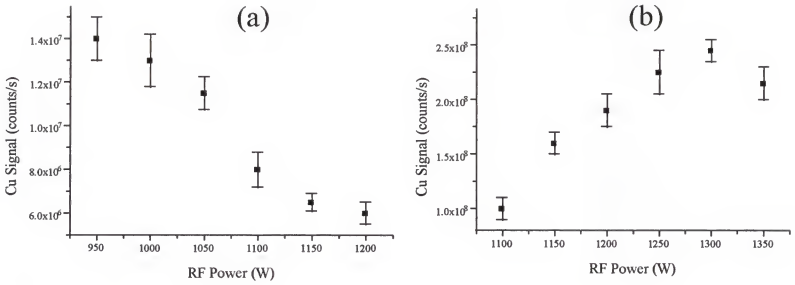


Figure 3-2. Effect of RF power on Cu signal for (a) dry and (b) wet plasmas.

Although background levels were higher, wet plasma operation was preferred for most LA-ICP-MS measurements. This was because it provided a convenient means for tuning the ion optics, gave better sensitivity and precision, and was useful in calibration studies as discussed in Chapters 4, 5, and 7. Tuning of the ion optics in the dry plasma mode involved continuously ablating a sample and adjusting the ion lenses to maximize the signal from a matrix element. For multielement work, a mid-mass element was chosen for tuning. Because the amount of material ablated by each laser shot varied and different size particles were being introduced to the ICP-MS, laser ablation signals tended to be noisier than those originating from nebulized solutions. The highly fluctuating signal made tuning of the ion optics difficult.

With the wet plasma, solution-based analytes could be used for tuning. This made tuning much easier since the signal was more stable. The major requirement for the applicability of solution-based tuning was that analytes in the solution aerosol behaved similar to those in laser ablated solid particles. Because of the high temperature of the ICP and the constant plasma conditions (i.e. solution was continuously introduced whether ablating or not), this appeared to be the case (Figure 3-3). These plots demonstrated that analyte signals from laser ablated NIST 611 glass (Co, Ni, Cu, Sr, and Ba) and a nebulized 20 ppb solution (Mg, Al, Mn, Co, Ni, Cu, Zn, Sr, and Ba) optimized at similar RF powers. In addition, all analytes optimized at the same RF power. Similar behavior was observed for soils, ceramics, and metallic alloys. This behavior was critical for the use of solution-based calibration for the analysis of solids, as will be discussed in Chapter 4.

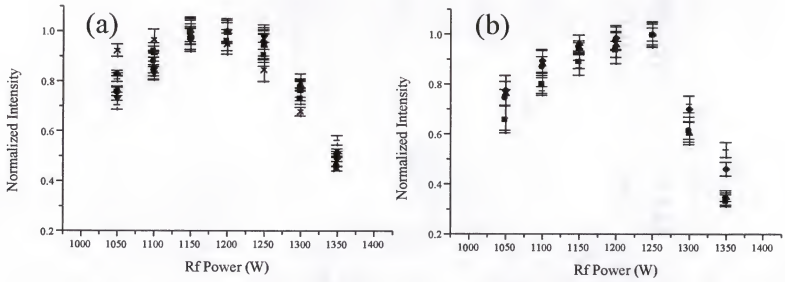


Figure 3-3. Effect of RF power on analyte signals for (a) solution and (b) laser ablated glass.

Table 3-2. Comparison of sensitivity and precision for wet and dry plasmas. NIST 611 glass

| | Mn | Ni | Cu | Zn | Sr |
|---|---|---|---|---|---|
| **Sensitivity-Dry (cps/ppm)** | 26 | 130 | 49 | 10 | 41 |
| **Sensitivity-Wet (cps/ppm)** | 3180 | 1050 | 1590 | 170 | 1660 |
| **Precision[a]-Dry (% rsd)** | 4.8 % | 16 % | 9.4 % | 13 % | 13 % |
| **Precision[a]-Wet (%rsd)** | 4.9 % | 8.9 % | 7.1 % | 5.6 % | 5.9 % |

[a] For precision measurements, analyte signals were normalized by the signal from Co.

The sensitivity and precision of LA-ICP-MS measurements was different for wet and dry plasmas. Table 3-2 compares the sensitivity (signal/ppm) and precision (% rsd) of laser ablation measurements for several elements in NIST 611 glass with both plasma operating modes. The concentration of analytes was around 500 ppm in the glass sample. The results indicated that much higher sensitivity was obtained with a wet plasma.

Several workers have studied the effects of water in the ICP and found that the presence of some amount of water provided higher excitation than the complete absence of water (56, 57). This is related to the presence of hydrogen produced from the dissociation of water. The thermal conductivity of hydrogen is about ten times that of argon, resulting in greater energy transfer in the ICP (56). There is obviously an optimum amount of water that should be added to the plasma. The quantity of water introduced to the plasma could be controlled by adjusting the temperature of the spray chamber. When the spray chamber was cooled, water condensed on the walls, resulting in smaller quantities of water being introduced to the plasma. The effect of spray chamber temperature on analyte signals was studied and the results for Ba are shown in Figure 3-4a. An increase in ion signals with decreasing spray chamber temperatures was observed for all analytes studied (Be, Mg, Co, In, Ba, Pb, and U). In addition, the decreased solvent loading resulted in lower oxide levels as shown for ArO (Figure 3-4b). The level of oxides for Ba and U were also studied and showed a decrease of about a factor of two between 25 °C and 0 °C. Unfortunately, some background species ($Ar_2$ and ArN) actually increased slightly with decreasing spray chamber temperatures.

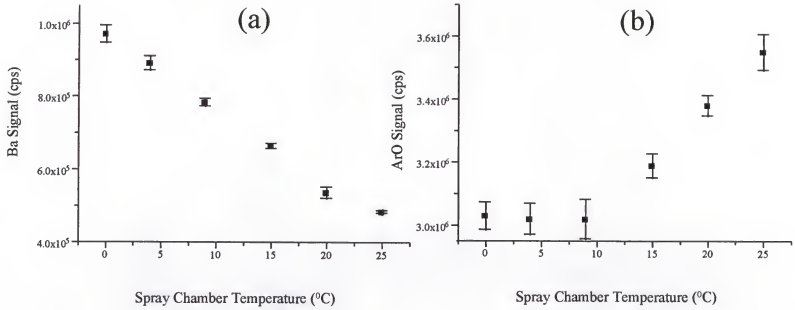


Figure 3-4. Effect of spray chamber temperature on (a) Ba and (b) ArO signals.

As indicated in Table 3-2, the precision of LA-ICP-MS measurements improved with wet plasma operation. The reason for poorer precision in dry plasma measurements was not entirely clear; however, it could be related to the different ablation chamber flow rates. The lower flow rates associated with wet plasma conditions allowed for more mixing of the ablation products from successive laser shots and produced more stable signals. For dry plasma, less mixing occurred and signal fluctuations were greater in magnitude. Because the quadrupole MS is a scanning instrument and spends a finite time at each mass, highly fluctuating signals can lead to reduced precision when measuring several isotopes. This will be illustrated more clearly in the consideration of scan times later in this chapter.

Another potential benefit of the lower ablation chamber flow associated with wet plasma operation was that it probably introduced smaller particles to the ICP. The fraction of material transported through the transfer tubing as a function of flow was estimated (Figure 3-5). The simple model (58) used in these calculations was based on uncharged spherical silica particles and assumed that gravitational settling (rather than convective diffusion) was the dominant loss mechanism. Arrowsmith and Hughes studied the entrainment and transport of laser ablation products produced from Mo metal (59). They determined that ~90 % of the products were entrained, ~40 % were transported to the ICP, and concluded that the major loss mechanism was gravitational settling. Because of differences in flow rates, tubing length, and ablation material, different values would be expected for the present work. As demonstrated in Figure 3-5, a significantly different particle size distribution would be transported to the ICP. For example, 5 μm particles would not be transported to the ICP in the low flow case, but

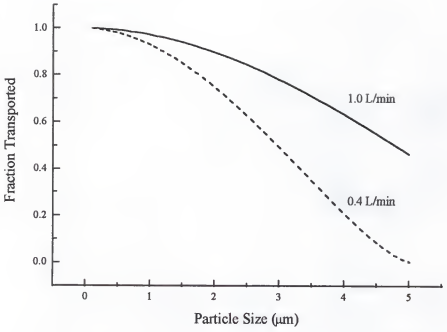


Figure 3-5. Calculated transport efficiency for silica particles at 0.4 L/min. and 1.0 L/min. Ar flow rates.

nearly 50 % of these particles would be transported with the higher flow rates associated with dry plasma operation. This is especially important considering that studies have indicated that particles >3 μm are not completely vaporized and excited in the ICP (60, 61). Thepresence of these particles could lead to selective removal of more volatile species in the ICP, resulting in inaccurate measurement of bulk concentrations. The particle sizes produced from laser ablation are dependent on numerous factors, including laser pulse duration, wavelength, irradiance, repetition rate, and physical properties of the material. Studies have indicated that a wide range of particle sizes (tens of nanometers to tens of micrometers) are produced during the ablation process (19, 21, 59).

Based on the comparison of wet and dry plasmas, all subsequent work was performed in the wet plasma mode. Although the increased level of some interferences was a drawback, the overall gain in analytical performance made it preferable. Interferences were usually not a problem at most masses; however where they were, another isotope of the element of interest was usually available. For example, $^{57}Fe$ could be measured instead of $^{56}Fe$, although with a loss in sensitivity due to differences in natural abundance.

Scan Parameters and Internal Standardization

The scan parameters (number of channels, dwell time, and number of passes) and data acquisition mode determined the total scan time for a measurement and played an important role in the accuracy and precision of LA-ICP-MS measurements. The number of channels refers to the number of discrete masses measured by the detector. In this system, a total of 4096 channels are available. Dwell time refers to the amount of time spent at each of these discrete locations (channels). The number of passes is simply the

number of times that the region or regions of interest are scanned over and averaged during a measurement.

A procedure which combined the relative merits of both peak jumping and scanning was used in the majority of this work. It involved scanning over a selected region of interest (1 amu/peak) and then rapidly jumping to the next region of interest for scanning, and so on. This allowed for the acquisition of true peaks, and therefore time was spent only on regions of interest. Both peak height and peak area measurements were used. Precision was similar for both types of measurements; but as expected, peak area measurement produced lower detection limits.

The total measurement time for laser ablation analyses was typically around one minute (300 shots @ 5 Hz). This was chosen to provide relatively rapid analyses, but with enough laser shots and mass ablated to introduce a representative portion of the sample to the ICP-MS. The amount of material ablated was dependent on the laser irradiance and sample type, but was typically in the range of 2-50 ng per shot. It was important to determine appropriate scan parameters for providing accurate and precise measurements.

For these studies, NIST 611 glass was ablated and nine different isotopes ($^{43}$Ca, $^{55}$Mn, $^{59}$Co, $^{60}$Ni, $^{63}$Cu, $^{88}$Sr, $^{107}$Ag, $^{138}$Ba, and $^{165}$Ho) were measured on the multiplier detector. For each isotope, 16 channels were measured with dwell times of 2, 8, 16, 32, and 64 ms. The number of passes (128, 32, 16, 8, and 4) was adjusted so that the same amount of time spent at each mass (~4 s). All measurements were normalized with an internal standard ($^{43}$Ca) to account for differences in mass ablated during and between measurements. The average % rsd for the measurements was 3.8 % (2 ms), 3.5 % (8 ms),

5.8 % (16 ms), 7.4 % (32 ms), and 8.4 % (64 ms). The latter dwell time represented the minimum dwell time that could be used with the faraday detector. These results clearly indicated the benefit of using short dwell times and a large number of passes to average out fluctuations in the laser ablation signal. Dwell times of 2 to 4 ms were used in all subsequent multielement laser ablation measurements.

The use of an internal standard ($^{43}Ca$ in the above measurements) was important for providing reasonable levels of precision. This was because a variable amount of material was ablated due to differences in laser power (20 % rsd for n = 15 laser shots), the nonlinearity of the ablation process (18), and the changing sample morphology (crater formation). To account for these variations, the signal from a matrix element was commonly measured. An important assumption was that the analytes and internal standard were distributed the same over the sampled area, and that they exhibited similar transport to, and excitation in the ICP. Internal standardization measurements typically improved the precision by a factor of two or so. This improvement was greater in some cases, for example, with soils and particulate samples. In these cases, the absolute signals would routinely vary by a factor of three or more. In addition, when analyzing multiple samples, it was difficult to ensure identical focusing of the laser beam with respect to the sample surface. Internal standardization provided a convenient means of mass normalization and eliminated the need to precisely control the position of the sample with respect to the focused laser beam.

Sampling Strategy

Initial work with the LA-ICP-MS system was confined to single spot measurements. The temporal profile of the $^{28}Si$ signal from a glass sample obtained by

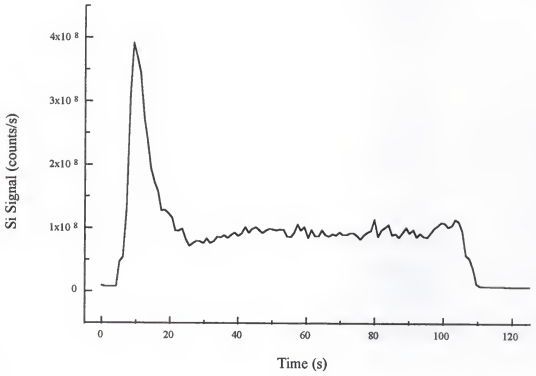


Figure 3-6. Temporal profile of Si signal from glass obtained with repetitive pulsing at a single spot.

repetitively firing the laser at a fixed location is shown in Figure 3-6. The benefits of repetitive pulsing, as opposed to single shot measurements, was that it allowed material from successive ablations to mix. This provided a continuous laser ablation signal. The MS could be repetitively scanned and information on the bulk sample was obtained. Typically, the initial signal was higher and then fell off to a lower "steady-state" level after 20 or 30 s. For this reason, a scan delay of 30 s was utilized in single spot measurements to minimize any bias resulting from measuring signals in the initial region where they changed very significantly, since the MS spent a finite time at each mass.

To determine whether the drop in signal was related to signal suppression or simply differences in the ablation efficiency, integrated measurements of smaller numbers of shots were performed. The laser was fired 50 times and the integrated $^{28}Si$ was measured. This was repeated in sets of 50 up to a total of 300 shots. Figure 3-7 indicates that the large initial signal was the result of a larger mass ablated rather than signal suppression. In addition, the laser was focused both above and below the laser surface to see if this had any effect on the observed behavior. Regardless of the laser focus, a larger mass was initially ablated and then a relatively constant amount was produced. This was not surprising since the first laser shots were incident on a flat surface; whereas, all subsequent shots were directed at the crater formed in the sample.

To take advantage of the higher initial ablation yield, the instrumentation was modified to allow for translation of the sample at 15 μm/s while the laser was repetitively fired. Faster translation rates tended to produce more erratic signals and also required that the direction of the stage be changed more often because of the limited sample width. As expected, translation resulted in improved sensitivity because of the higher ablation

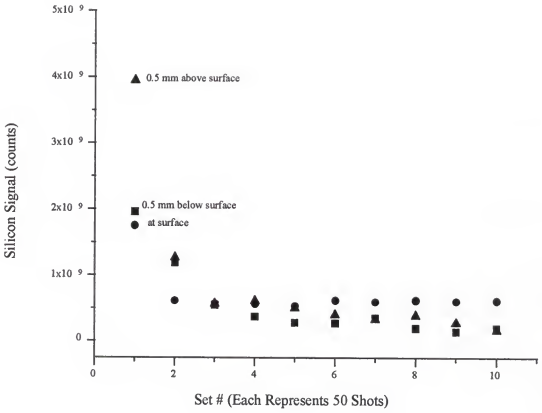


Figure 3-7. Si signal as a function of shot number.

rate. The effect was greatest with pressed powder samples since the craters formed in the surface were deeper, resulting in relatively rapid defocusing of the laser beam. A comparison of craters produced from single spot and translation sampling is shown in Figure 3-8. Measurements of the ablation depth and volume for these craters will be discussed in Chapter 5. Another potential benefit of translation is that a larger area on the surface can be sampled, minimizing the effects of local lateral heterogeneity. A drawback is that a smaller surface layer is removed when translating and surface contamination and/or heterogeneity can be problematic. This will be demonstrated with glass samples in Chapter 4.

(a)

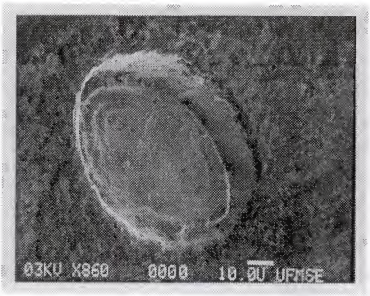


(b)

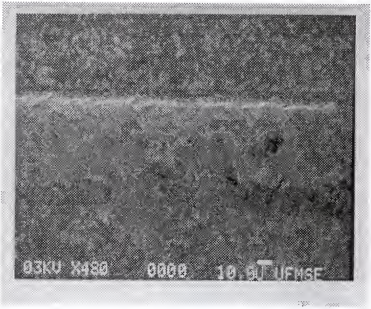


Figure 3-8. Laser produced craters in silicon nitride with (a) single spot and (b) translation sampling.

# CHAPTER 4
# ANALYSIS OF GLASS SAMPLES

## Introduction

Numerous studies on the analysis of glasses by laser ablation inductively coupled plasma mass spectrometry (LA-ICP-MS) can be found in the literature. These studies deal with a wide range of applications, from elemental fingerprinting of crime scene evidence (62) to the use of glasses as calibration standards for geological materials (63-66). In the glass industry, as the number of formulations and applications of glass materials continues to grow there is an increased demand for rapid, accurate, and precise determinations of the concentrations of elemental constituents (67). Direct methods of analysis are preferred because of the difficulty in digesting these materials. Dissolution generally consists of three steps: (1) treatment with HF; (2) further oxidation by addition of $HNO_3$, $HClO_4$, or $H_2O_2$; and (3) final addition of HCl or $HNO_3$ (68). When digesting in an open vessel, silica is lost by formation of volatile $SiF_4$. An alternative to wet chemistry is melting the sample with a suitable flux, such as sodium hydroxide or lithium metaborate. The major problem with this method is the production of high salt concentrations, which can lead to significant matrix effects and/or block the nebulizer and ICP-MS sample cone (68). Because of the difficulties and time required for both methods, LA-ICP-MS is an attractive alternative; LA eliminates the need for extensive sample preparation and also offers the potential for information on the spatial distribution of elemental constituents.

Glasses have been studied in this work for several reasons. They provided a relatively homogeneous, analyte-rich matrix for characterization of the LA-ICP-MS system. They were certified for several elements and therefore provided immediate feedback on the suitability of non-matrix matched calibration strategies. As previously mentioned, this was of particular interest because of the lack of matrix-matched standards for many materials of interest (e.g. ceramics). The use of solution-based calibration for the analysis of glasses will be addressed in this chapter and some of the important findings discussed.

## Experimental

The LA-ICP-MS system has been described previously (Chapter 3). Table 4-1 lists the typical ICP-MS operating conditions. The laser was operated at 5 Hz with energies ranging from 0.1-0.7 mJ. Both single spot and line sampling were used.

NIST glass samples (611, 612, 614, and 617) were used in these studies. These are synthetic Si, Na, Al, and Ca glasses which have been spiked with 61 different elements at nominal concentrations of 500 ppm (NIST 611), 50 ppm (NIST 612), 1 ppm (NIST 614), and 0.02 ppm (NIST 617). They are in the form of 1-3 mm thick discs.

For the solution-based calibration studies, a 10 ppm multielement standard (High Purity Standards Charleston, SC) was diluted with deionized water and Optima-grade $HNO_3$ (Fisher Scientific, St. Louis, MO) was added to bring all solutions to 2 % $HNO_3$. Concentrations of the standards ranged from 1 to 50 ppb. A 2 % $HNO_3$ blank was continually introduced during laser ablation analyses via a glass Y-connector at the base of the ICP torch. In this way, identical plasma conditions were maintained whether an ablated solid or nebulized solution was being introduced.

Table 4-1. ICP-MS operating conditions.

| | |
|---|---|
| Rf Power | 1200 W |
| Coolant gas flow rate | 15 L/min |
| Auxiliary gas flow rate | 0.9 L/min |
| Nebulizer gas flow rate | 0.6 L/min |
| Ablation chamber flow rate | 0.4 L/min |
| Solution uptake rate | 1.0 mL/min |
| | |
| Scan Conditions | |
| Faraday Scans (major elements) | |
| Scan range per isotope | 1 amu |
| Number of passes | 32 |
| Number of channels per amu | 8 |
| Dwell time | 64 ms |
| Multiplier Scans (minor elements) | |
| Scan range per isotope | 1 amu |
| Number of passes | 128 |
| Number of channels per amu | 16 |
| Dwell time | 4 ms |

The ion lenses, nebulizer gas, and RF power were optimized using the ($^{115}$In) signal from a 1 ppm solution (measured on Faraday). Both the Faraday and multiplier detectors tuned at almost identical ion lens settings; therefore, either detector could be used with the optimized settings. An ICP-MS response curve (Figure 4-1) was generated for typical tuning conditions using a multielement solution. The absolute sensitivity (number of ions detected / number of atoms introduced) was calculated for nine different analytes (Be, Mg, Ni, Co, In, Ce, Pb, Bi, and U) which encompassed the mass range from 9 amu (Be) to 238 amu (U). The resulting plot indicated that the instrument was most sensitive for mid-mass analytes and fell off for low and high mass analytes. It was investigated whether tuning with a low ($^{24}$Mg) or high mass isotope ($^{208}$Pb) had any effect on the instrumental response curve. No significant differences were observed.

Typical scan parameters are listed in Table 4-1. For most multielement analyses, a total scan time of 60-80 s was used. This resulted in the averaging of 300-400 laser shots per measurement. A 30 s delay was typically used before the start of data acquisition as discussed in Chapter 3. Both peak height and peak area measurements were used. Peak heights were measured directly using the SOLA instrument control software. Peak area measurements were performed by importing the ASCII scan files into a spreadsheet program for integration of the spectra. Typically, 8 channels were integrated for each peak. Temporal profiles of analyte signals were generated by sequentially and repetitively monitoring masses of interest. This feature was incorporated into the SOLA software suite; however, due to problems in the program, only a limited number of masses could be monitored.

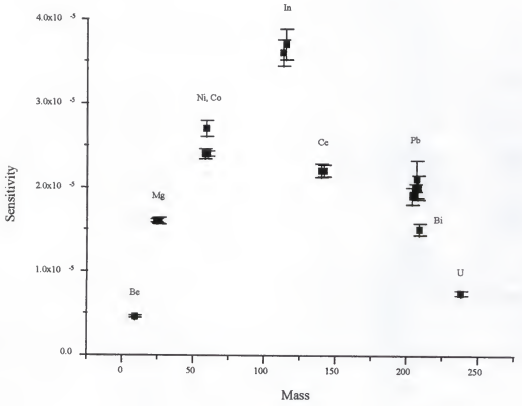


Figure 4-1. ICP-MS response curve generated by nebulization of a 1 ppm multielement solution. Sensitivity refers to the number of ions detected per number of atoms introduced to the ICP-MS.

Calibration Procedure

The feasibility of using solution standards for the semiquantitive analysis of solid materials has been studied previously (38, 67, 69-71). Hager (71) developed a model that used response factors determined from solution nebulization and modified them based on element-dependent volatilization efficiencies. This work reported accuracies of only +/- 50 % for aluminum, steel, and copper standards. The technique does not appear to be a general method because ablation of nonmetals is likely to produce molecular species, such as oxides and silicates. In addition, a large fraction of the ablated material transported to the ICP is solid particles that have undergone solid-liquid-solid, rather than solid-monatomic gas, phase changes (69). The use of dual-sample introduction appears to be a more promising alternative for analyzing materials where suitable calibration materials are not available. Its utility has been demonstrated for geological samples (38, 67, 70) and metals (69).

The calibration procedure used in this work involved measuring the intensity of a single isotope for each element of interest (including an internal standard) in solution standards and determining relative sensitivity factors (RSF's). The RSF is defined in equation (4-1), where E represents the element of interest and IS represents the internal standard.

$$\text{(4-1)} \quad RSF(E,IS) = \frac{\text{Sensitivity(E)}}{\text{Sensitivity(IS)}} = \frac{\text{Intensity(E)}}{\text{Concentration(E)}} \bullet \frac{\text{Concentration(IS)}}{\text{Intensity(IS)}}$$

If (a), identical plasma and mass spectrometer conditions prevail when nebulized calibration solutions or laser ablated solid particulates are being introduced to the ICP-MS (see Figure 3-2) and (b), the ablation material is an accurate representation of the bulk material, then RSF's obtained from solutions and solids will be equal, i. e.

(4-2) $RSF(E/IS)_{solution} = RSF(E/IS)_{solid}$.

Provided that the concentration of the internal standard is known in the solid of interest, the RSF's can be used to calculate the concentration of analytes from the expression

(4-3) $$Concentration(E)_{solid} = \frac{Intensity(E)_{solid}}{Intensity(IS)_{solid}} \bullet \frac{Concentration(IS)_{solid}}{RSF_{solution}}.$$

A major requirement of this solution-based methodology is that the concentration of some element (the internal standard) must be known prior to analysis. This can either be measured by some complementary technique, such as x-ray microanalysis (EPMA), or determined from the stoichiometry of the solid. This is obviously a limitation of the technique and a potentially useful method for overcoming this limitation is discussed in Chapter 6. Typically, a minor isotope of a major matrix constituent is chosen as the internal standard. In the analysis of these certified glass materials, $^{43}Ca$ was found to be the most suitable internal standard because of relatively low levels of interference at this mass, and because signals could be measured with the multiplier detector. Signals greater than $10^6$ counts/s (cps) resulted in saturation of the electron multiplier detector, which was exclusively used for the multielement analysis of trace elements in these glasses.

## Results

### Fractionation

The production of ablated material that is an exact representation of the original sample is essential in non-matrix-matched calibration of bulk materials. For inhomogeneous samples, this requires that enough material is removed so that local concentration variations in the solid are averaged out. For samples that are homogeneously distributed on the scale of sampling, the major problem is fractionation

of species during the ablation process. Internal standardization can generally account for differences in mass ablated both within and between matrices; however, fractional ablation is more of a problem since fractionation causes enhancements or reductions in relative analyte signals. Several workers have studied the role and extent of fractionation in laser ablation measurements (69, 72-78). These investigations have revealed the importance of laser wavelength, irradiance, and sample characteristics in determining the extent of ablative fractionation. In addition, transport fractionation has been revealed as a source of fractionation as well (75).

Two mechanisms have been proposed for ablative fractionation: volatilization of non-refractory elements from sample areas outside the bulk ablation area; and zone refinement, where elements within the molten zone surrounding the ablation crater undergo selective migration into the laser ablation spot. Recent work has indicated that the latter mechanism is the most likely source of fractionation, since the extent of fractionation correlated with melting points of the element compounds in the sample (75, 78). If the former mechanism was dominant, the boiling point or vapor pressure of the element compound would be critical.

The effect of laser irradiance and wavelength on elemental fractionation has been studied as well (69, 78). Cromwell and Arrowsmith (69) reported that the Pb/Cu ratio produced from a brass sample with UV laser ablation was one order of magnitude higher with lower laser irradiances ($< 1.3 \times 10^8$ W/cm$^2$) than at higher irradiances ($> 10^9$ W/cm$^2$). They attributed the increased fractionation at lower irradiances to the increased volume of molten sample relative to the bulk ablation volume. Recently, Figg and Kahr (78) studied the effect of laser irradiance, as well as laser wavelength, on ablative

fractionation in glass samples. They reported much higher fractionation in the case of ablation with 1064 nm and 532 nm wavelengths, compared to 266 nm. This agrees with earlier studies that compared ablation behavior for IR and UV lasers (76, 77).

In the case of UV lasers, the primary means of material removal is by direct laser interaction with the surface for the duration of the laser pulse. The initiation of the laser induced plasma occurs in less than 1 ns; however, the UV beam is not significantly absorbed and the role of the plasma in material removal is insignificant (77). With an IR laser, the direct interaction only lasts a fraction of the laser pulse duration since the plasma is highly absorbing at this wavelength. The plasma is heated by the laser energy and the primary means of material removal is by the plasma-material interaction (77). This produces local heating of the sample, resulting in greater fractionation of more volatile species.

In this work, the effect of laser irradiance on relative analyte signals was studied to determine if fractionation was occurring, and if so, to what extent. This was essential if the goal of accurate quantitative measurements was to be realized. In this study, NIST 611 glass was repetitively ablated at 5 Hz with laser pulse energies of ~ 0.5 mJ. The sample was not moved, since this would maximize local heating of the sample and induce fractionation. The focus of the laser was adjusted over a range of 2 mm to adjust the irradiance at the sample surface. The laser spot size, as determined by the surface craters, ranged from 40 μm to 200 μm. Signals for eleven elements ($^{11}B$, $^{55}Mn$, $^{59}Co$, $^{85}Rb$, $^{88}Sr$, $^{89}Y$, $^{90}Zr$, $^{133}Cs$, $^{182}W$, $^{208}Pb$, and $^{209}Bi$) were acquired over ~ 500 laser shots. The ratios of intensities to the $^{55}Mn$ intensity were determined to see if any changes were observed over the range of irradiances. Mn was chosen because it's oxide melting point (oxides

should be dominant species in glass) was intermediate for those elements studied. Table 4-2 lists the oxide melting points for several elements in the glass sample.

The results for these measurements are given in Figure 4-2. The intensity ratios have been normalized to their value at the highest laser irradiance (~ $5x10^8$ W/cm$^2$). Therefore, the relative change in composition can be determined by the deviation from a value of one. In Figure 4-2 (a), elements with oxide melting points lower than Mn are plotted and in (b), elements with higher oxide melting points are plotted. Based on these results, significant differences in the composition of the ablated material were not observed for the low melting point elements until very low irradiance values (< $5x10^7$ W/cm$^2$). Below this value, fractionation of more volatile elements occurred (as much as 2 times in the case of Bi). Since an irradiance of $5x10^7$ W/cm$^2$ was near the ablation threshold, visual observation of the laser-induced plasma could be used as a guide to ensure that the laser irradiance exceeded this value. The presence of a visible laser spark on the sample surface could then be used as a guide to ensure representative sampling of these elements in glass.

The behavior of those elements with higher oxide melting points was more of a problem. The relative intensity of Co did not deviate significantly over the range of irradiances studied; however, this was not surprising considering the proximity of the oxide melting points for Co and Mn. The relative intensities of Y and Zr decreased for irradiances below ~$1.5x10^8$ W/cm$^2$, indicating that these more refractory oxides were not being ablated representatively. For some unknown reason, this trend was reversed at lower laser irradiances. Nonetheless, these studies revealed that at laser irradiances of $2x10^8$ W/cm$^2$ and greater, a reproducible ablation composition was produced. This was

Table 4-2. Oxide melting points.

| Element | Oxide Melting Point (°C)[a] |
|---|---|
| Bi | 180, 825 |
| Ag | 230 |
| Pb | 290-500, 886 |
| Cs | 400 |
| Rb | 400, 570 |
| B | 450 |
| W | 800-900, 1473, 1500-1600 |
| Co | 895, 1795 |
| Cu | 1235, 1326 |
| Mn | 1564 |
| Zn | 1975 |
| Ni | 1984 |
| La | 2307 |
| Y | 2410 |
| Sr | 2430 |
| Ca | 2614 |
| Zr | 2700 |

[a] from reference 79

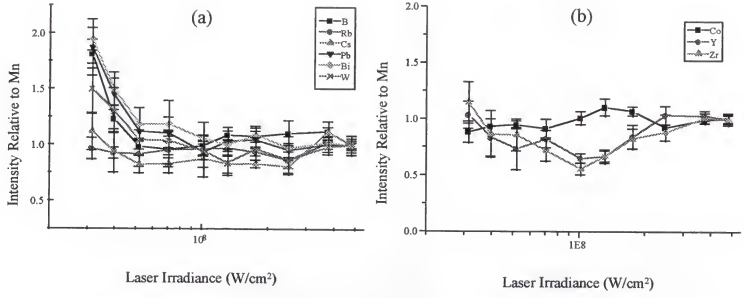


Figure 4-2. Effect of laser irradiance on relative analyte signals for elements with (a) lower oxide melting points and (b) higher oxide melting points than Mn.

important considering that slight changes in the laser focus, resulting from crater formation, surface roughness, or the analysis of samples with small differences in height would not significantly affect LA-ICP-MS results. The case is different when spatial information is sought, since the crater diameter and depth are dictated by the laser irradiance. In this instance, ablative fractionation would be more significant and proper consideration would have to be given to account for this effect if analyte concentrations were sought.

The consistency of the ablation product did not guarantee that it was truly representative of the bulk material. Some melting of the glass material did occur as evidenced in Figure 4-3, which compares the unablated glass surface (a) to the inside of a laser produced crater (b). This and all other scanning electron micrographs (SEM's) were taken with a JEOL 35CF electron microscope. The representativeness of the ablation product would be assessed from solution calibration results.

Solution-Based Calibration

In the discussion on the solution calibration procedure, it was stated that accurate results could only be obtained if two criteria were met: (1) identical plasma conditions should be maintained for both solution and ablated solid analysis and (2) the ablation process should produce a representative subsample. The latter aspect was recently discussed. The criterion of identical plasma conditions was speculated to exist based on similar RF optimization behavior for ablation and solution measurements (see Figure 3-2). This point was more clearly illustrated when RSF's obtained from a 10 ppb multielement solution and laser ablated NIST 611 glass with the ICP-MS operated in

(a)

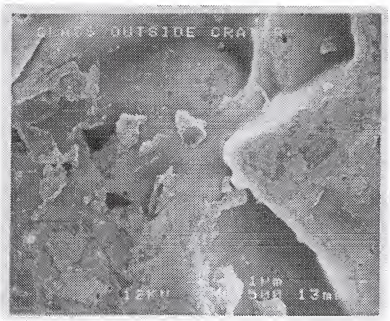

(b)

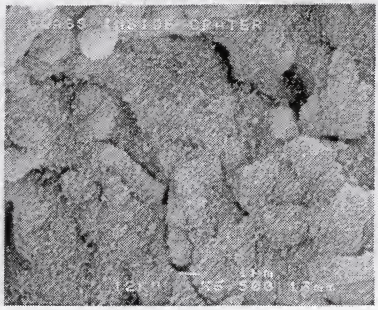

Figure 4-3. Comparison of (a) unablated and (b) ablated glass surface.

Table 4-3. Comparison of RSF's for solution and laser ablation measurements.

| Element | Solution RSF[a] (sd)[b] | LA-Wet RSF[a] (sd)[b] | LA-Dry RSF[a] (sd)[b] |
|---|---|---|---|
| Mn | 1.00 (.03) | 0.87 (.04) | 0.41 (.02) |
| Ni | 0.20 (.01) | 0.19 (.02) | 3.1 (.5) |
| Cu | 0.51 (.01) | 0.44 (.04) | 0.46 (.04) |
| Zn | 0.064 (.005) | 0.046 (.003) | 0.14 (.02) |
| Sr | 0.607 (.02) | 0.45 (.03) | 1.6 (.2) |

[a] relative to Co

[b] standard deviation for n=5 measurements

both the dry and wet plasma (dual sample introduction) modes were compared (Table 4-3). All results were relative to Co, which was present in the glass at around 390 ppm. The RSF's obtained from solution and those for laser ablation with dual sample introduction mode agreed very well with one another (5-28 %), especially considering that a noncertified minor element was being used as the internal standard. This indicated that under the experimental conditions used, the glass matrix was representatively sampled. Laser ablation measurements with a dry plasma resulted in considerably different RSF's compared to solutions (10-1450 %), even though identical laser sampling conditions were employed. The discrimination, therefore, arose in the ICP-MS and indicated the importance of matched plasma conditions for obtaining accurate results.

The need to measure an internal standard was somewhat restrictive; however, it was extremely beneficial in providing stable and reproducible measurements. This was not only in terms of correcting for differences in mass ablated, but also in accounting for instrumental drift. This point is clearly illustrated in Figure 4-4. In this plot, the average intensities of $^{59}Co$ and $^{60}Ni$ from a 50 ppb solution were plotted over a series of fifteen scans (1 min/scan). Even though the solution was being continuously introduced at the same rate, a significant decrease in signal levels was observed. It was later determined that this was due to an aging detector. The use of absolute intensities would have been meaningless in this case, but the relative intensities remained stable (1.2 % rsd) since all isotopes exhibited the same behavior.

Similarly, it was observed that RSF's obtained from solutions did not change significantly over time due to similar ICP-MS tuning conditions. This was somewhat

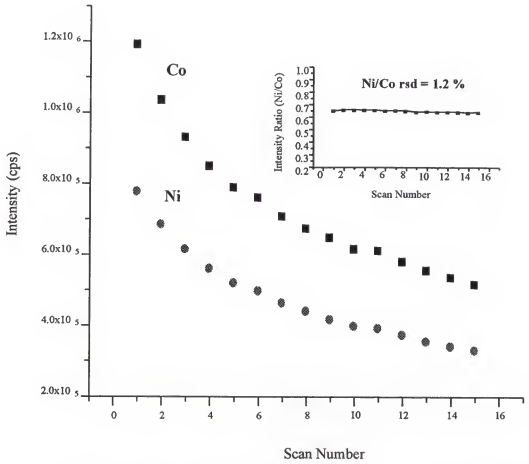


Figure 4-4. Ni and Co intensities as a function of scan number (time). Inset shows the ratio of the two intensities.

surprising, even though the same tuning procedure was used each time the instrument was run. The implication was that RSF's measured on one day were reliable for considerable periods of time if no major instrumental modifications were made. To illustrate this point, the element concentration values from a NIST 611 glass determined by the solution calibration procedure were compared for three different days. The solution RSF's determined on the first day were used to calculate analyte concentrations (see Equation 4-3) on that day, the next day, and one month later. The results are given in Table 4-4 and indicate that significant differences in accuracy were not observed over this period of time. The precision (% rsd, n=5 replicates) of the measurements was typically 10 % or better. Considering that a trace element (Sr) was used as the internal standard, the accuracy and precision of these measurements was quite good. In later measurements, an isotope of a major matrix constituent ($^{43}Ca$) was used as the internal standard. For all of these measurements, ablation and data collection were performed at five different fixed locations on the glass surface. After this time, the instrumentation was modified to allow for translation of the sample during ablation. A comparison of the results obtained for these two different sampling modes will be presented.

Spot Sampling Versus Line Sampling

Sample translation during ablation was investigated because of several potential advantages. Sample translation should have provided higher signals since a partially fresh surface was being ablated by each laser shot and would be expected to give more representative sampling for inhomogeneous materials. In addition, reduced fractionation should have resulted since the laser was not defocused from crater formation and

Table 4-4. Results for NIST 611 glass based on solution calibration.

| | Cert. Conc.[a] (ppm) | Meas. Conc. (ppm) Day 1 (% difference) | Meas. Conc. (ppm) Day 2 (% difference) | Meas. Conc. (ppm) Day 30 (% difference) |
|---|---|---|---|---|
| **Mn** | 485 | 470 (-3.1 %) | 454 (-6.3 %) | 354 (-27 %) |
| **Ni** | 458.7 | 489 (6.6 %) | 438 (-4.4 %) | 339 (-26 %) |
| **Co** | (390) | 389 (-0.2 %) | 447 (14 %) | 312 (-20 %) |
| **Cu** | (444) | 366 (-17 %) | 350 (-21 %) | 342 (-23 %) |
| **Zn** | (433) | 312 (-28 %) | 295 (-32 %) | 269 (-37 %) |
| **Rb** | 425.7 | 399 (-6.3 %) | 413 (-3.0 %) | 434 (1.9 %) |
| **Tl** | (61.8) | 50.0 (-19 %) | 66.5 (7.6 %) | 72.1 (17 %) |
| **Pb** | 426 | 366 (-14 %) | 415 (-2.6 %) | 464 (9.0 %) |
| **U** | 461.5 | 352 (-24 %) | 445 (-3.7 %) | 497 (7.8 %) |

[a] Values in parentheses are not cerified

localized sample heating would be less significant since the same area was not continuously ablated with the high powered laser.

For a typical 1 minute analysis (300 laser shots), translation of the sample at 15 μm/s produced signals that were on average 2 to 3 times higher than those obtained from a single spot. The dimensions of a typical single spot and translated sample crater were measured with an optical microscope. For single spot sampling, the crater was estimated to be 75 μm wide and 120 μm deep. If a parabolic crater was assumed, this corresponded to a total ablated mass of 830 ng (2.2 ng/shot). For translation, the crater was 50 μm wide, 15 μm deep, and 900 μm long (assumed from 15 μm/s x 60 s). If a parabolic trough was assumed, this corresponded to a total ablated mass of 1350 ng (3.8 ng/shot). This provided further evidence that translation resulted in higher ablation efficiencies. The exact magnitude of signal enhancement could not be inferred from these measurements, since the sample was typically ablated for 100 shots (20 s) before signals were acquired. It was previously shown (Figure 3-8) that the ablation efficiency decreased significantly after the first 50 shots when single spot sampling was used.

NIST 611 glass was analyzed to assess the homogeneity of the material and to determine if sampling strategy had any effect on the accuracy of solution calibration based measurements. For this study, scans were made at different spots (25 total) on the sample or at different lines (5 scans/line) produced from translating the sample. Several isotopes ($^{43}Ca$, $^{55}Mn$, $^{59}Co$, $^{60}Ni$, $^{63}Cu$, $^{88}Sr$, $^{208}Pb$) were measured for a total acquisition time of one minute. Ca served as the internal standard in these measurements, since it was a major matrix constituent (12 % CaO). The RSF's determined from both sampling methods were compared with RSF's obtained from a solution containing 20 ppb of all the

elements of interest, except for Ca, which was present at 2 ppm. This closely matched the ratios of trace element to Ca in the glass sample. The results for Mn, Co, Cu, and Sr are presented in Figure 4-5. The translation values were significantly higher for Mn and Co, slightly higher (statistically significant at 95 % level) for Cu and Ni (not shown), and almost identical for Sr and Pb (not shown). Where differences did occur, spot sampling measurements were more accurate as evidenced by their proximity to the solution results. The most likely reason for these discrepancies was either inhomogeneity in the sample or the presence of fractionation.

Examination of the glass surface with scanning electron microscopy revealed the presence of a significant amount of redeposited particles (Figure 4-6). For comparison, the top of this picture contains areas that had been previously ablated. After ablation, the sample surface was wiped clean to remove any redeposited material. It was thought that these redeposited particles might possibly be enriched or depleted in certain elements and could influence the laser based RSF's, making them vary more significantly compared to the solution value. The effect would be more significant for translation analyses since areas where particles were redeposited would be continuously sampled as the laser probed the surface. Also, because the surface layer sampled was smaller with translation the proportion of redeposited material to fresh material would be greater in this case. In order to investigate these potential sources of variation, a larger set of elements was studied and sampling was performed in a way that would maximize any effects due to sampling of redeposited material.

In this study, elements encompassing a wide range of oxide melting points (see Table 4-2) were measured since it has been shown that the extent of fractionation

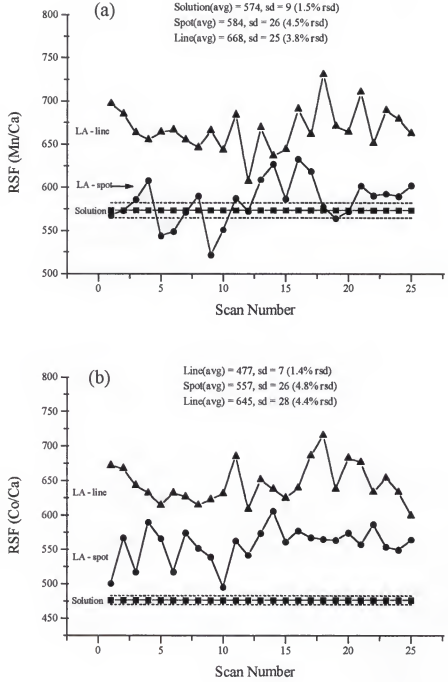


Figure 4-5. Comparison of results for spot and line sampling for Mn, Co, Cu, and Sr.

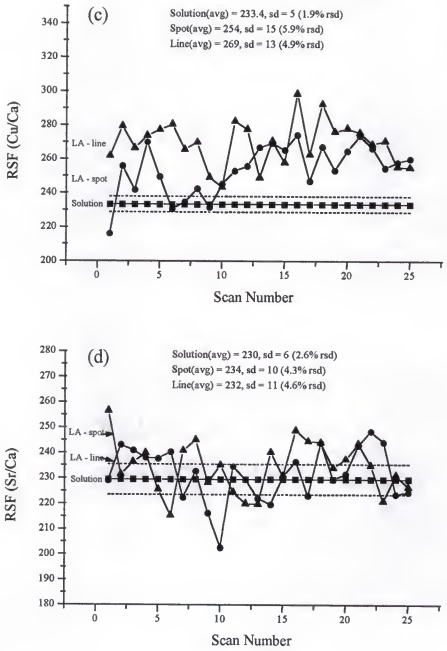


Figure 4-5 continued.

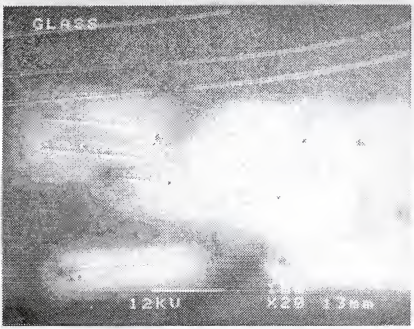


Figure 4-6. SEM of glass surface after ablation.

correlated with this property (75, 78). The isotopes used were $^{43}Ca$, $^{55}Mn$, $^{59}Co$, $^{60}Ni$, $^{63}Cu$, $^{66}Zn$, $^{88}Sr$, $^{90}Zr$, $^{107}Ag$, $^{139}La$, and $^{208}Pb$. The oxide melting points ranged from 230 °C for Ag to 2700 °C for Zr. Both single spot and translation measurements were performed as previously described. In order to maximize the proportion of redeposited material sampled, additional analyses were performed close to previous ablation tracks at the same laser energy (0.5 mJ) and with lower energies (0.1 mJ). The use of lower laser energies should result in the sampling of an even smaller surface layer. To ensure that any differences observed at low energies were due to the sampling of redeposited particles, analyses were also performed at a location well removed from any previous ablation craters.

Table 4-5 summarizes the results obtained for glass ablated with single spot sampling, translation sampling, and translation sampling through areas with significant amounts of redeposited material. All of these measurements were performed with a laser energy of 0.5 mJ. Significant differences (> 10 %) between spot and translation sampling were observed for Mn, Co, Zr, and La. A statistically significant difference (at 95 % level) was also observed for Ag. RSF's for Mn and Co increased with line sampling, while those for Zr, La, and Ag decreased. No major difference between translation measurements was observed in this study, indicating that the particles did not have any effect on the results at this laser energy. The differences observed for spot and translation sampling could not be explained on the basis of fractionation. If fractionation was occuring, it should have been more prevalent with spot sampling because localized heating would be more likely in this case. Since Ag and Zr had the lowest and highest oxide melting points, respectively, they should have displayed opposite behaviors. The

Table 4-5. RSF's obtained from various sampling strategies.

| | Single Spot RSF[a] (sd)[b] | Translation RSF[a] (sd)[b] | Translation-redep. RSF[a] (sd)[b] |
|---|---|---|---|
| **Mn** | 530 (20) | 610 (30) | 620 (30) |
| **Co** | 510 (20) | 580 (30) | 580 (30) |
| **Ni** | 122 (5) | 121 (5) | 123 (5) |
| **Cu** | 230 (9) | 240 (10) | 250 (10) |
| **Zn** | 56 (3) | 53 (3) | 54 (3) |
| **Sr** | 217 (5) | 218 (8) | 216 (7) |
| **Zr** | 139 (5) | 113 (5) | 113 (2) |
| **Ag** | 120 (5) | 112 (4) | 115 (5) |
| **La** | 101 (6) | 89 (3) | 84 (4) |
| **Pb** | 1.6 (.1) | 1.8 (.2) | 1.8 (.2) |

[a] relative to $^{43}Ca$

[b] standard deviation (n = 15 measurements)

RSF for Ag should have increased for spot sampling (observed), while Zr should have remained stationary or decreased slightly (opposite observed). In addition, Mn and Co exhibited the largest RSF changes, even though these elements did not possess melting points significantly different from elements (e. g. Cu, Zn, and Ni) where no changes in RSF's were observed. The differences observed were most likely the result of small-scale inhomogeneity in the glass samples. Measurements performed with a lower laser energy supported this notion.

A comparison of RSF's (Figure 4-7) obtained for spot sampling with a laser energy of 0.5 mJ and translation sampling with energies of 0.5 mJ and 0.1 mJ revealed significant differences. In this plot, RSF values were normalized to solution RSF values; therefore, the accuracy of the measurements was readily apparent. For example, a value of 1.1 indicated a 10 % error, 1.2 a 20 % error, and so on. The low energy measurements were performed both near a previous ablation track and well beyond any previously ablated areas. No significant difference between these measurements was observed, providing more proof that the particles did not affect the accuracy of measurements. For Ag and Cu, these low energy measurements resulted in significantly higher RSF's compared to higher energy measurements. This was almost certainly due to inhomogeneity since an even smaller surface layer was being sampled in these cases. It could have resulted from surface contamination, but this was unlikely since only these two elements demonstrated this behavior. Likewise, if fractionation were at fault differences would have been observed for other elements as well.

The results clearly indicated the importance of introducing a representative portion of the sample during analysis. Single spot sampling resulted in better accuracy

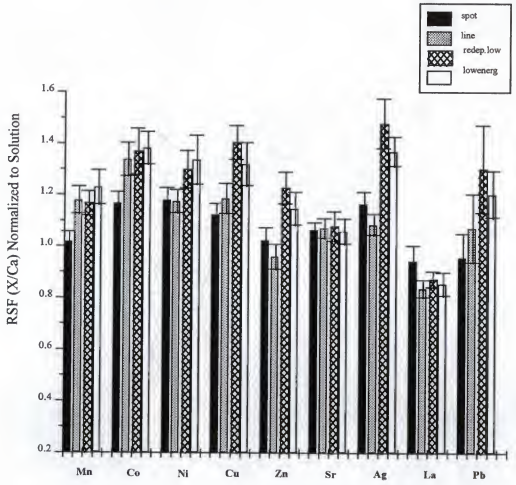


Figure 4-7. Comparison of RSF's obtained for spot sampling (0.5 mJ) and line sampling (0.5 mJ and 0.1 mJ).

(average of 9.5 %) than translation mesurements (average of 14 %) for glass, since it was less affected by in-depth inhomogeneity. Sampling depths were around ten times higher with the former. The precision (% rsd) of the measurements was less than 5 % for both sampling modes. Lateral inhomogeneity was not a problem in either case, due to the relatively large crater diameters (50 μm or greater). This behavior should not be generalized since the sampled volumes, homogeneity, and physical characteristics of the sample all play a role in determining the most suitable sampling strategy.

## Conclusions

Calibration using standard solutions and dual sample introduction was shown to provide reasonably good accuracy (+/- 10 %) for trace elements in NIST glass samples. Detection limits ($3\sigma$) were less than 1 ppm for all elements studied. The effects of ablative fractionation were studied and it was determined that at irradiances > $2x10^8$ $W/cm^2$, representative sampling was achieved. Sampling strategies were compared and it was determined that spot sampling produced more accurate measurements for the glass samples. Translating the sample produced higher signal intensities; however, local heterogeneity was more problematic because a smaller surface layer was sampled in this mode. Ablated mass was estimated to be a couple of ng's per shot.

# CHAPTER 5
# ANALYSIS OF SILICON NITRIDE CERAMIC BEARINGS

## Introduction

There is considerable interest in using silicon nitride ($Si_3N_4$) bearings for a wide variety of applications. Such interest results from the unique chemical and physical properties which these ceramics possess. In comparison to conventional steel bearings, silicon nitride bearings offer high speed and acceleration capability because of their low density, extended temperature capability, longer lifetimes and lower wear rates, excellent corrosion resistance, and the ability to operate under conditions of marginal lubrication (80). This combination of qualities has led to investigations of silicon nitride bearings for use in high speed, high temperature applications, such as in the aerospace industry.

The physical and mechanical properties of ceramic materials are influenced by trace element impurities (81-84). Therefore, comprehensive trace element characterization, in terms of both the bulk composition and spatial distribution of elements, is required for ceramic materials if they are to be used in demanding environments. Digestion procedures have been used for ceramics with analysis of the resulting solution by several techniques, including ICP-AES/MS (85, 86) and Flame AAS (85). These procedures are difficult and time consuming, due to the resistance of ceramic materials to chemical attack. Wet chemical procedures can also introduce contaminants, and they only provide information on the bulk sample and tell nothing of the distribution of elemental constituents in the ceramic.

Direct sampling methods are preferred for the analysis of compact ceramics. Several reviews discuss the methods currently used for analyzing ceramic materials (81, 82). Characterization of ceramics on both the bulk and micro scale is required in many cases. Most often, several complementary techniques are necessary to provide this information. LA-ICP-MS is extremely well suited for the bulk characterization of ceramic materials, and also possesses the capability of providing spatial information on the μm scale. The suitability of laser ablation results from the ability to sample essentially any type of material with little to no sample preparation. The major obstacle to the use of LA-ICP-MS for the quantitative analysis of ceramic materials has been the lack of suitable standard reference materials. In some cases, synthetic ceramic standards were created for analyzing ceramics with LA-ICP-MS (87, 88); however, these were designed to analyze a specific material. It would be valuable to develop methodology that would allow for the accurate analysis of a wide range of ceramics. This issue was the driving force behind the investigation of solutions for calibration of solid materials, as discussed in Chapter 4.

In this chapter, use of the solution calibration methodology for reliable quantitative elemental analysis of silicon nitride ceramic bearings will be presented. In addition, the use of NIST glasses for calibration of silicon nitride ceramics will be discussed. The results obtained from the two methods were compared to one another, and with results obtained by electron probe microanalysis (EPMA). Ablation craters have been characterized using both profilometry and scanning electron microscopy. The detection efficiency of the LA-ICP-MS system was estimated based on the profilometry results.

## Experimental

The LA-ICP-MS system (Chapter 3) and typical operating conditions (Chapter 4) were previously discussed. The laser was operated at 5 Hz, with pulse energies of 0.7 mJ. Both single spot and translation sampling were used in this work. Typical analysis times were 60 to 80 s (signals averaged over 300 to 400 laser shots).

Silicon nitride bearings (NBD-100 Cerbec, East Granby, CT) were mounted in epoxy and cut with a diamond blade wafering saw to obtain a flat surface. They were then polished to a 1 μm finish. These sample preparation steps were required for the EPMA analysis only. Laser ablation analyses could be performed directly on the intact bearing.

The solution calibration methodology was presented in Chapter 4. For the analysis of silicon nitride, it would have been preferred to use a minor isotope of silicon ($^{29}$Si or $^{30}$Si) as the internal standard directly; however, large interferences at these masses resulted in saturation of the multiplier detector. Magnesium was chosen as an alternative, since it was present at significant levels (1000s of ppm) in the samples, and also possessed an isotopic pattern which allowed for its measurement using both the Faraday ($^{24}$Mg – 79 % abundance) and multiplier ($^{25}$Mg – 10 % abundance) detectors. The analytical procedure involved measuring $^{28}$Si and $^{24}$Mg with the Faraday detector and determining the concentration of magnesium in the sample based on the solution RSF($^{24}$Mg/$^{28}$Si). The concentration of silicon (60 %) was estimated from sample stoichiometry. All other elements (minor and trace) were measured with the multiplier detector and the concentrations were determined from sensitivity factors relative to $^{25}$Mg.

In the glass-based calibration work, a National Institute of Standards and Technology glass was used (NIST 611). Cobalt was used as the internal standard for these studies, since its concentration in the glass was known and magnesium's was not. The calibration procedure was similar; RSF's (analyte/$^{59}$Co) obtained from the glass matrix were used to calculate the concentrations of analytes in the silicon nitride bearing.

Ablation craters were characterized using an Alpha-Step 500 profilometer (Tencor Instruments, Santa Clara, CA) and a JEOL 35CF scanning electron microscope (SEM). For the SEM's, the silicon nitride samples were attached to mounts with carbon paint and coated with AuPd to provide a conductive surface. EPMA of the silicon nitride bearings was used for comparison with LA-ICP-MS results. For these analyses, a carbon coating was used since this resulted in lower background levels. The work was performed on a JEOL Superprobe 733.

## Results

### Identification and Distribution of Elements in Silicon Nitride

A complete mass scan of the silicon nitride bearings (NBD 100) used in this study resulted in the identification of 26 elements (Mg, Al, Ca, Sc, Ti, Cr, Ni, Co, Cu, Sr, Y, Zr, Mo, Nb, Ag, Cd, Sn, Ba, La, Ce, Pr, Nd, Ta, W, Pb, and Bi). Although no attempt was made to quantify all of these elements, their estimated concentrations ranged from the hundreds of ppb level to thousands of ppm. For comparison, a newer grade of bearing material (NBD 200) was analyzed and contained much lower levels of impurities, with only the sintering aid (Mg) having a high concentration (> 100 ppm). Only ten elements were present at high enough levels to be detected with the LA-ICP-MS system. For this

reason, the NBD 100 bearings were chosen for all subsequent work since they provided a more analyte-rich sample.

For LA-ICP-MS to be used for bulk analysis of the ceramic bearings, it was essential that the small surface layer sampled (~ 5 μm) on the exterior of the bearing be representative of the bulk material (Figure 5-1). This was tested by analyzing the interior and exterior surfaces of a cut bearing. The measured concentrations of all analytes were almost identical within the measurement uncertainty, indicating that the relatively small volume sampled by laser ablation of the surface provided information on the bulk specimen. The SEM (Figure 5-1) revealed that the ablation process resulted in both melting and fracturing of the silicon nitride surface. Melting was evidenced by the presence of redeposited spherical particles around the ablation craters, as well as by a comparison of the unablated (Figure 5-2 (a)) and ablated (Figure 5-2 (b)) silicon nitride surface. A discussion of the particles produced, and their origins, from laser ablation of ceramic, glass, and soil samples will be presented in Chapter 6. Fracturing of the silicon nitride surface was evidenced by the small step-like features outside of the main ablation track.

As mentioned in the experimental section, an isotope of magnesium was chosen as the internal standard for most of the quantitative measurements. A requirement for the use of internal standardization for obtaining accurate results is that the analyte and internal standard be distributed similarly over the area sampled, and that they exhibit similar behavior in transport to and excitation in the ICP. This was tested, albeit on a limited basis, by measuring the temporal response of the $^{25}Mg$ and $^{63}Cu$ signal over a period of 90 s, while the laser was repetitively fired (Figure 5-3). The two signals

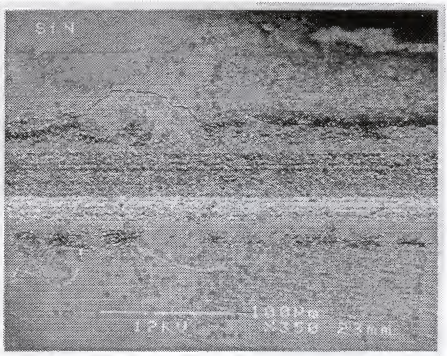


Figure 5-1. Scanning electron micrograph of a laser ablation track in silicon nitride. The sample was translated at 15 μm/s. SEM was taken with the sample tilted at 50 degrees.

(a)

(b)

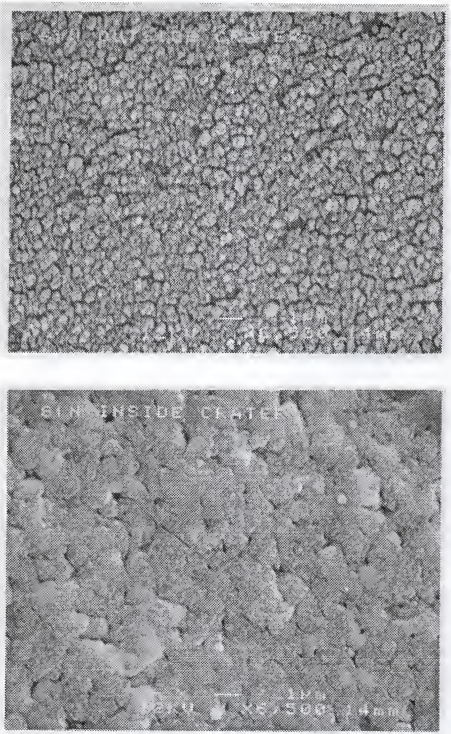


Figure 5-2. Scanning electron micrographs of (a) unablated and (b) ablated silicon nitride surface.

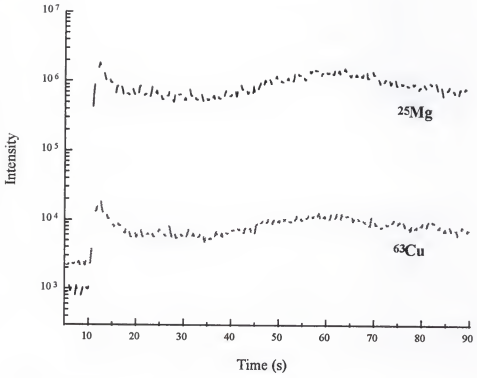


Figure 5-3. Temporal profiles of Mg and Cu signals from silicon nitride.

correlated very well with one another, and partially justified the use of $^{25}Mg$ as the internal standard for quantitative measurements of trace constituents in the ceramic. Additionally, the distribution of magnesium and titanium was studied in the silicon nitride bearing. Signals for these two elements were measured from 24 different locations on the sample. The % rsd of the elemental ratios (Ti/Mg) was 10 %, indicating that titanium and magnesium were distributed similarly over the surface of the bearing.

Results from Solution- and Glass-Based Calibration

Results for the analysis of a silicon nitride bearing using RSF's obtained from standard solutions are given in Table 5-1. For comparison, results obtained with EPMA are provided for the three most concentrated elements (Mg, Co, Al) present in the silicon nitride. Because of the inferior sensitivity of EPMA, these were the only elements detectable in the sample by this method. The agreement between the techniques was excellent, suggesting that the use of solutions for calibration is effective for the analysis of ceramic materials. The precision of the techniques was similar, with % rsd's (n=10 for LA and n=5 EPMA) ranging from 2 to 18 %.

In addition to solution-based calibration for silicon nitride ceramics, the use of NIST 611 glass as a calibration standard was investigated. In this work, a second bearing was analyzed. Similar to the procedure used for solutions, RSF's (analyte/Co) obtained from the glass sample were used to determine the concentration of analytes in the ceramic sample. A smaller number of elements was used in this study because of the limited number of certified elements in the glass. In several cases, the noncertified values provided by NIST were used (Co, Cu, and Zn). The results are presented in Table 5-2

Table 5-1. Comparison of results obtained with LA-ICP-MS using solution calibration and EPMA.

| Analyte | LA-ICP-MS[a] Concentration (ppm) | EPMA[b] Concentration (ppm) |
|---|---|---|
| Mg | 7200 +/- 400 | 7300 +/- 500 |
| Co | 1420 +/- 60 | 1300 +/- 200 |
| Al | 2230 +/- 60 | 2400 +/- 50 |
| Ni | 79 +/- 6 | |
| Cu | 28 +/- 3 | |
| Sr | 8 +/- 1 | |
| Mo | 12 +/- 1 | |
| Ba | 16 +/- 1 | |
| La | 7 +/- 1 | |
| Nb | 38 +/- 6 | |
| Y | 18 +/- 2 | |

[a] Confidence interval (95 %) based on 10 measurements.
[b] Confidence interval (95 %) based on 5 measurements.

Table 5-2. Comparison of results using solution and glass-based calibration.

| Analyte | Results from solution RSF's (ppm)[a, b] | Results from glass RSF's (ppm)[a, b] | Results from glass sensitivities (ppm)[a] |
|---|---|---|---|
| Mn | 103 +/- 3 | 123 +/- 5 | 120 +/- 15 |
| Co | 1540 +/- 60 | 1380 +/- 90 | 1400 +/- 200 |
| Ni | 58 +/- 2 | 65 +/- 3 | 63 +/- 8 |
| Cu | 9 +/- 2 | 10 +/- 2 | 9 +/- 2 |
| Zn | 9.2 +/- 0.7 | 13 +/- 1 | 13 +/- 2 |
| Sr | 7 +/- 1 | 9 +/- 1 | 8 +/- 2 |

[a] Confidence intervals (95 %) based on 10 measurements.
[b] Results for Co based on Co/Ni relative sensitivity factor (RSF).

and demonstrated that similar results were obtained for both solution- and glass-based calibration.

The last row of this table represents an extension of the use of glasses for calibration. In this case, the absolute analyte sensitivites (intensity / concentration) from laser ablated glass were used with a correction factor to account for differences in the ablated mass between the glass and ceramic sample. The value of the correction factor was determined by measuring the $^{28}Si$ from both samples and taking into account the differences in nominal silicon concentration of the samples. It was determined that the ablated mass was four times greater for the glass than the ceramic, under similar sampling conditions. Not suprisingly, the measured analyte concentrations agreed with those obtained by the other methods. The precision of these measurements was worse (12-15 % rsd), since the measurements involved non-normalized sensitivity values obtained from glass.

It would have been beneficial to measure an isotope of silicon along with the analytes to directly compensate for variations in ablated mass; however, this was not feasible with the present system. The use of solutions produced high background levels (mainly oxides) and precluded the measurement of $^{29}Si$ and $^{30}Si$ with the multiplier detector. This could be remedied, at least in part, by incorporating a desolvation apparatus to further decrease the solvent loading; however, this was not attempted in this study. Alternatively, independent measurements of ablated mass, such as the use of acoustic waves generated by the ablation process (89), or measurement of the scattering signal produced by the mobilized ablation product (90) could prove useful for the analysis of ceramic materials with glass-based calibration. The use of independent mass

normalization would eliminate the need for internal standardization and provide a more powerful method for analyzing ceramic materials based on glass standards. Light scattering for mass normalization with glass, ceramic, and soil samples will be presented in Chapter 6.

Measurement of Mass Ablated and Estimation of System Efficiency

Profilometry and weight loss measurements were performed on the silicon nitride samples to determine the amount of material removed by the ablation process and to determine the efficiency of the LA-ICP-MS system. As previously addressed (Chapter 3), sample translation resulted in a larger mass removal rate and subsequently higher sensitivities. Profilometry measurements (Figure 5-4) on the craters shown in Figure 3-8 indicated that the volume ablation rate was nearly double in the case of sample translation compared to single spot sampling (3 pL/s compared to 1.6 pL/s). These corresponded to mass ablation rates of 9 ng/s and 5 ng/s, respectively. The higher ablation rate was due to the fact that a partially pristine surface was being ablated by each laser shot with translation of the sample. The ablated masses agreed reasonably well with those obtained by weighing the sample before and after approximately 50,000 laser shots. The observed ablation rates were used to determine a system efficiency for the sintering aid Mg (Mg ions detected / Mg atoms removed). In these measurements, the $^{24}Mg$ signal was continuously monitored during the ablation process. The total integrated signal was then divided by the estimated mass of Mg ablated. Efficiency of detection for Mg was estimated to be 1 in 500,000. The efficiency of detection for analytes is a function of the ablation process, transport process, ionization in the ICP, and mass spectrometer response.

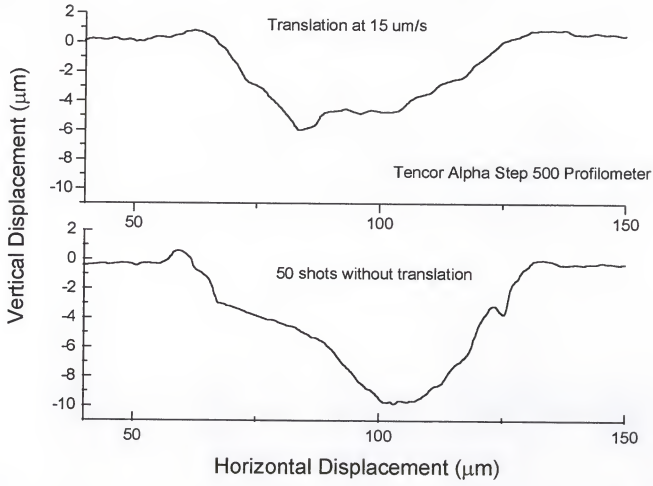


Figure 5-4. Profilometry traces of craters in silicon nitride with and without translation of the sample.

## Conclusions

The use of both solution and glass-based calibration has been demonstrated for the analysis of silicon nitride bearings. The results obtained from solutions were verified with a complementary technique, EPMA. Use of glasses for calibration provided similar results to those obtained from solutions and may prove useful in the future for a wide variety of ceramic materials. A large number of standard glass materials are presently available, making them very attractive as potential calibration materials for ceramics. The ability to independently measure differences in the mass ablated for glass and ceramics would greatly improve the utility of glass-based calibration.

# CHAPTER 6
# INVESTIGATION OF LIGHT SCATTERING FOR MASS NORMALIZATION IN LA-ICP-MS

## Introduction

To account for variations in ablated mass and improve the precision and accuracy of laser ablation measurements, the signal from a matrix element is commonly used as an internal standard (38, 45, 46, 70). This improves the precision, provided the spatial distribution of the internal standard and the analyte are similar, and the elements behave similarly in terms of ablation, transport, and ionization in the ICP. To improve the accuracy of LA-ICP-MS measurements, it is also required that the concentration of the internal standard be known. In many cases, this information is not readily available or can vary significantly, such as with many geological materials and multi-layered ceramics. In such instances, there is a need for independent measurement of the mass ablated.

Several techniques that independently measure differences in the mass ablated have been investigated (89-91). Pang *et al.* demonstrated that the acoustic wave generated by the ablation process could be used to normalize analyte signals in LA-ICP-MS (89). Their work resulted in modest improvements of the precision compared to the non-normalized signals from steel and aluminum alloy samples. Other work has involved measurements on the mobilized ablation products. Richner *et al.* measured the light loss caused by scattering from ablated material as it passed through a cylindrical

glass tube (91). They reported that normalization of analyte signals from cast iron samples based on this technique was comparable to the use of an internal standard. Similarly, Tanaka *et al.* used the light scattering signal produced from the transported aerosol to normalize analyte signals (90). In their work with zirconium alloys, they also reported an improvement in precision that was comparable to internal standardization.

In this work, the use of light scattering for normalization with several matrices, including brass, glass, soil, and Macor® (Corning Glass Works, Corning, NY) ceramic has been investigated. It is demonstrated that a simple light scattering system can be used for mass correction with a variety of materials. Normalization based on light scattering results in improved precision of LA-ICP-MS measurements; however, this method of normalization is not as good as the use of an internal standard. The major strength of the present technique is that it did not require any knowledge of the sample homogeneity or concentrations of elements. This makes it potentially useful for the accurate analysis of inhomogeneous samples as well as those for which standards are not readily available. This latter aspect has been studied by examining the effectiveness of the light scattering system for normalization between different types of samples (glass, ceramic, and soil).

## Experimental

The LA-ICP-MS instrumentation (Chapter 3) and operating conditions (Chapter 4) were previously described. One difference was the use of a smaller ablation cell. It consisted of a 3 cm i.d. Plexiglas tube with a quartz window for transmission of the UV laser beam. The total volume of the new ablation cell was ~ 50 $cm^3$. The smaller cell was used to produce a denser ablation aerosol for larger scattering signals.

The scattering cell (Figure 6-1) was placed in-line with the transport tubing. It was placed approximately 0.5 m from the ablation chamber. The body of the scattering cell was a 4-way Swagelok®(Crawford Fitting Co., Solon, OH) connector with a 1.5 mm hole drilled in the top for measurement of the particle scattering at 90°. Smaller angle viewing would result in higher scattering intensities, but the present arrangement was chosen for its simplicity. Windows of the scattering cell were mounted at Brewster's angle on 3 cm extension arms made of stainless steel tubing. The arrangement produced less stray-light scatter from the windows and interior of the cell. A 3 mW polarized HeNe laser (Aerotech, Inc., Pittsburgh, PA) operating at 632.8 nm was used as the scattering source in these measurements. To improve the quality of the output beam, the laser was spatially filtered before the scatter cell with an adjustable iris.

An end-on photomultiplier tube (R647, Hamamatsu Photonics K.K., Japan) was used to collect the scatter produced as the ablation aerosol passed through the cell. The entire scatter assembly was enclosed in a light-tight box. An alternative arrangement, which would eliminate the need for darkness, would be to use an interference filter that would transmit only a very narrow region of light centered at the HeNe wavelength. Signals from the PMT were amplified by a current to voltage amplifier (Keithley Instruments, Inc., Cleveland, OH) with a gain of $10^6$ V/A and a rise time of 100 ms. The amplifier output was fed to a computer interface module (Stanford Research Systems, Inc., Palo Alto, CA) which was triggered at 100 Hz. Normalization measurements were made by integrating the scatter signal over a given number of shots, as well as averaging the "steady-state" level produced during continuous ablation of translated samples for a total of 200 shots (40 s).

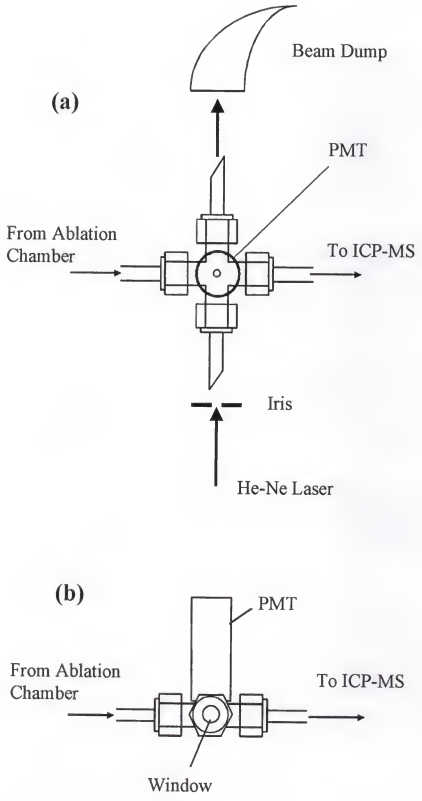


Figure 6-1. Schematic of light scattering set-up ((a) top view and (b) side view).

NIST glass (611, 612, 614, and 617) and brass (c1101, 1102, c1109, c1110) standard reference materials were used to assess the utility of the scattering system for normalization of analyte signals within a particular matrix. In the glass samples, the $^{88}Sr$ isotope was measured with the ICP-MS as well a minor isotope of a major matrix constituent ($^{43}Ca$) in order to compare the results from scatter normalization with those obtained by internal standardization. The concentration of Sr in the glasses ranged from 41.72 ppm to 515.5 ppm. For the brass samples, the $^{68}Zn$ isotope was measured. Concentrations of Zn in these standards ranged from 15.2 % to 30.3 %. In the inter-matrix studies, NIST 611 glass, NIST 2704 soil, and a Macor® ceramic disc were used. The soil samples were pressed into pellets, without the addition of a binder at a pressure of 35 MPa, for laser ablation analyses. In these studies, the $^{28}Si$ isotope was measured since silicon is the major matrix element in each of the matrices. The amount of silicon in the glass, Macor®, and soil was 34 % (nominal), 21.5 % (nominal), and 29.66 % (certified), respectively.

The nature of the particulate material produced from laser ablation of glass, soil, and Macor® samples was studied by collecting ablated material on 0.3 μm membrane filters (Millipore Corp., Bedford, MA). Because of the significant pressure drop created with the in-line filters, it was necessary to use a vacuum pump on the back side of the filter to eliminate flow restrictions. Flow conditions, identical to those used in the normalization experiments, were achieved by adjusting the pump valve and measuring the Ar flow rate with a rotameter. After collection, filters were glued onto mounts with conductive carbon paint and coated with AuPd for examination with a scanning electron microscope.

## Results

### Scatter Signal Normalization and Comparison with Internal Standardization

Initial experiments with the scattering system were performed to determine if the scattering signals correlated with signals from the ICP-MS. Figure 6-2 illustrates typical (a) scatter and (b) mass spectrometric signals obtained from 50 laser shots on NIST 611 glass. It should be mentioned that the actual transit time to the scattering cell was ~1 s, and ~3 s to the ICP-MS. The large number of spikes present in the scatter signal was assumed to be due to larger particles passing through the scatter cell based on visual observation. To evaluate the efficiency of the system for detecting changes in the mass removed, ablation was performed with different laser energies and focus positions. The total difference in mass ablated over these conditions ranged over approximately one order of magnitude. A plot of the average scatter and $^{28}Si$ mass signals (Figure 6-3) demonstrated that the two signals were highly correlated ($R = 0.98$). In this example, differences in the mass ablated were generated by changing the laser sampling parameters (i. e. focus and pulse energy); however, these differences occurred naturally over the series of glass standards under identical sampling conditions. This was probably due to differences in the surface characteristics of the glasses, since they were all completely opaque at 266 nm. Similar behavior has been reported by Mermet and co-worker in the laser ablation of glasses with a 266 nm Nd:YAG (92).

In the absence of normalization, differences in the mass ablated between the samples would not allow small changes in analyte concentration to be detected. This is illustrated by a series of calibration curves for Sr in NIST glasses (Figure 6-4), where in (a), the non-normalized analyte signals are plotted; in (b), the scatter normalized signals

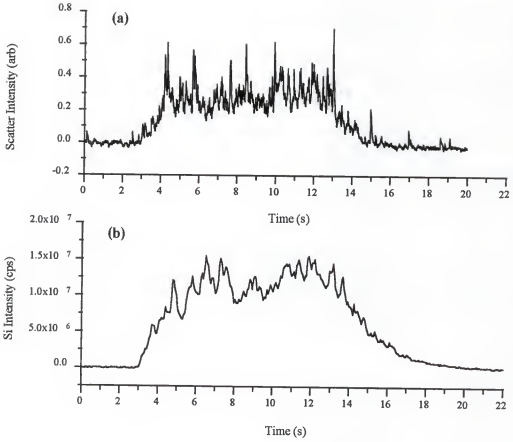


Figure 6-2. Plots of (a) scatter and (b) mass spectrometric signals obtained from 50 laser shots on glass surface.

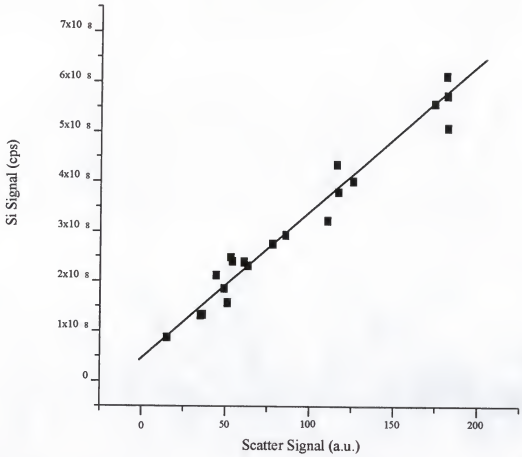


Figure 6-3. Correlation plot of mass spectrometric and scatter signals from NIST glass.

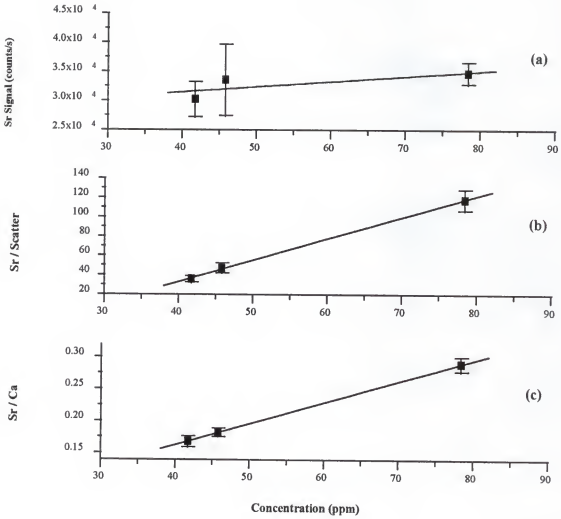


Figure 6-4. Calibration plots for Sr in NIST glass samples (a) without normalization, (b) with scatter normalization, and (c) with internal standardization.

are used; and in (c), the analyte signals are corrected by an internal standard ($^{43}Ca$). Without the use of normalization by scattering or internal standardization, a linear regression R value of 0.77 was obtained. R values obtained with the normalization techniques were both greater than 0.999. The precision of the scatter normalized measurements, for 5 replicates and 200 laser pulses/replicate was 5-12 % rsd. This was not as good as the precision obtained with an internal standard (3-6 % rsd); however, the use of light scattering is not limited to homogeneous samples, or samples in which a suitable internal standard is available. This includes samples where the major matrix constituents do not have a minor isotope, resulting in ion intensities which would saturate the multiplier detector, or the isotope is interfered with from a sample constituent or some background species. The precision of the non-normalized signals ranged from 5-19 % rsd.

Precision of the scatter normalized measurements was slightly worse than that reported by Tanaka *et al.* (90), although a direct comparison cannot be made because in the present work, a low energy UV laser was used for ablation; while in their work, a 150 mJ Nd:YAG operating at 1064 nm was used to ablate zirconium alloys. This should have resulted in significantly larger quantities being ablated, although the mass of material removed was not reported.

Although the main focus of the present work was to evaluate the effectiveness of scatter normalization with nonconducting matrices, NIST brass samples were also analyzed. Figure 6-5 demonstrates the use of scatter normalization for the calibration of Zn in these standards. The calibration plot exhibited a higher degree of correlation when the $^{66}Zn$ was corrected by the measured scatter signal (R = 0.999) as shown in (b), than

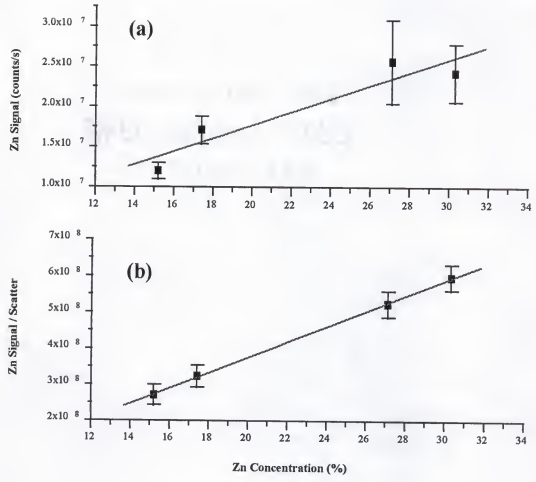


Figure 6-5. Calibration plots for Zn in NIST brass samples (a) without normalization and (b) with scatter normalization.

when the analyte signal alone was plotted (a) (R = 0.94). Precision of the measurements was 6-11 % rsd (n=5, 200 pulses/measurement) for the normalized signals and 8-20 % rsd for the non-normalized values. Not only did the use of light scattering improve the precision of the measurements within a given sample, but it also accounted for the different masses ablated between samples as evidenced by the improved fit of the regression line.

Comparison of Scatter Normalization for Glass, Soil, and Macor® Ceramic

A comparison of glass, soil, and Macor® was made to assess the utility of the scattering system for corrections of mass ablated between these matrices. This was initiated, in part, by the desire to use glass standards for the calibration of ceramic materials (Chapter 5). In Chapter 5, it was demonstrated that glasses could be used to analyze silicon nitride ceramic bearing, provided that differences in ablated mass were accounted for. To study whether light scattering could be used for mass normalization between matrices, a glass (NIST 611) disc, soil pellet (NIST 2709), and Macor® disc were ablated to investigate the relationship between mass removed and scattering signal.

Correlation plots, similar to Figure 6-3, are shown in Figure 6-6 for the three different matrices. In this figure, the MS signals have been normalized by the amount of silicon present in the samples to allow for a direct comparison of the matrices. Changes in the mass ablated were achieved by varying the energy of the laser. Slightly higher laser energies were used for the Macor® sample, since a smaller quantity of material was ablated for a given energy compared to the glass and soil samples. The laser energy ranged from 0.1 mJ to 0.7 mJ. Correlation between the scatter and MS signals was good for the glass (R = 0.94) and Macor® (R = 0.96) samples, but slightly worse for the soils

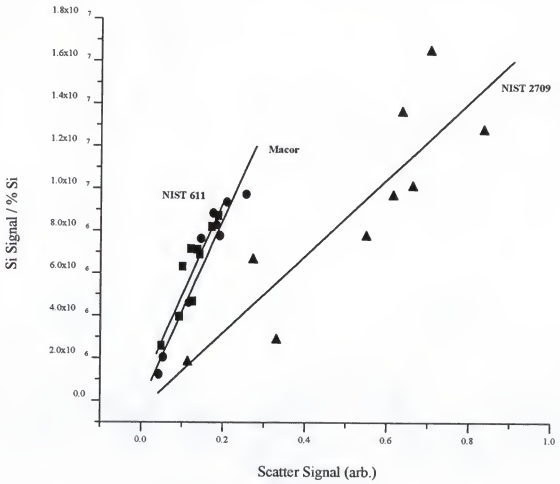


Figure 6-6. Correlation plot of mass spectrometric and scatter signals from glass, macor, and soil.

(R = 0.88). Most importantly, the plot indicated that the scattering signal effectively accounted for differences in the mass ablated between the glass and ceramic samples as evidenced by the proximity of the data points for these materials. The similar scatter-MS signal relationship of glass and Macor® is more clearly illustrated in Figure 6-7, where a single regression line could be drawn through the set of data points with an R = 0.97. The scatter-MS signal relationship was significantly different for the soils. In this case, a larger scattering signal was produced per unit of matrix removed, which resulted in the soil data points lying closer to the scatter axis.

The nature of the particulate matter produced from ablation of these materials helped explain the experimental results. Scanning electron micrographs (SEMs) of the collected particles are shown in Figure 6-8. The pictures clearly demonstrated that the particles produced from (a) glass and (b) Macor® were both smaller and more similar than those from the (c) soil samples. The similarity in particle sizes for these matrices allowed for effective mass correction based on the scattering signal. The larger particle sizes produced from the soil sample resulted in a significantly different Scatter-MS signal relationship. This difference was not surprising; however, the larger soil particles, to a first approximation, should have produced a smaller scatter signal per unit mass compared to the other matrices. The opposite behavior that was observed in this study was most likely due to the fact that the larger particles the scatter cell "saw" were not efficiently transported to the ICP, and would therefore not contribute to the MS signal. Transport efficiency as a function of particle size was discussed in Chapter 3. This is a limitation of the present system and could be alleviated by placing the scattering cell

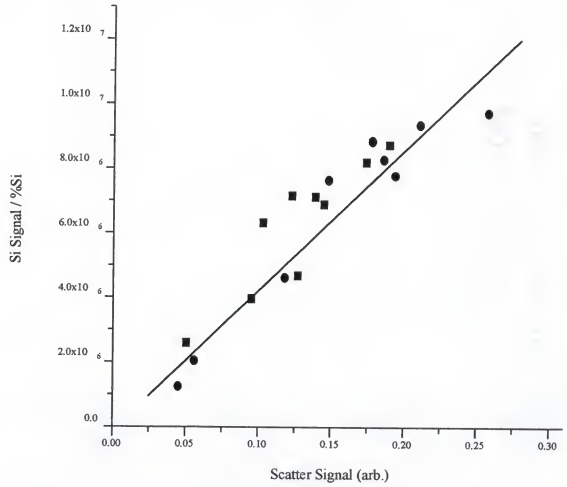


Figure 6-7. Correlation plot of mass spectrometric and scatter signals for glass (squares) and macor (circles).

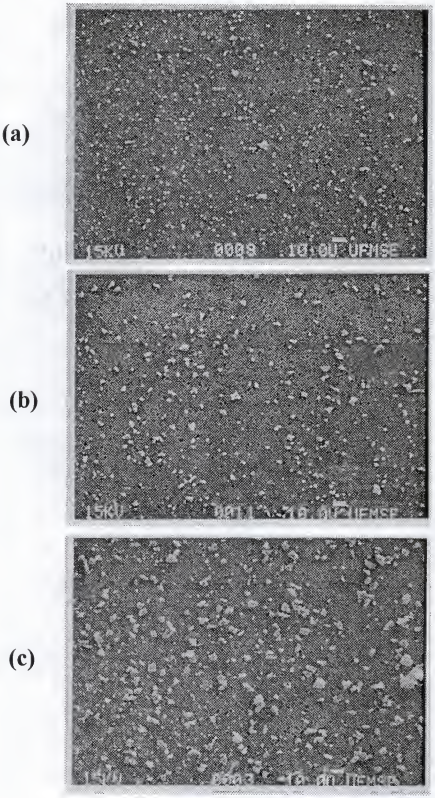


Figure 6-8. Scanning electron micrographs of particles collected for (a) glass, (b) macor, and (c) soil.

closer to the ICP torch, resulting in a more representative view of the material introduced to the ICP-MS.

Figures 6-9 (a-c) are higher magnification images of particles collected for glass, ceramic, and soil, respectively. Most of the particles produced from glass and Macor® were nearly perfect spheres. These were formed by cooling of liquid material and suggested that the bulk of the ablated material was melted and then explosively removed from the sample (93). Angular particles were also produced as a result of the mechanical and thermal shock of ablation, as well as a small amount of amorphous material that was most likely condensate from the gas phase. Such particle classifications have been described by other researchers as well (93, 94). The ablation product from soil was dominated by larger particles that resulted from mechanical and thermal shock, although each class of particle was seen. The greater presence of large particles was reasonable since these pressed pellets did not possess the mechanical rigidity of the glass and Macor® samples.

Weight loss measurements were performed for the glass and Macor® samples to verify that the mass ablated agreed with the experimental results. The samples were weighed before and after 40,000 laser shots at a laser pulse energy of 0.7 mJ. The average mass ablated for glass and Macor® was 16 ng/shot and 6.1 ng/shot, respectively. This agreed reasonably well with the scattering signals produced for ablation at this laser energy, and demonstrated that the scattering system was capable of measuring relatively small quantities of ablated material passing through the scatter cell. Scattering sensitivity could be improved with a smaller observation angle and/or a shorter wavelength laser; however, the present system was sufficiently sensitive and easily set-up.

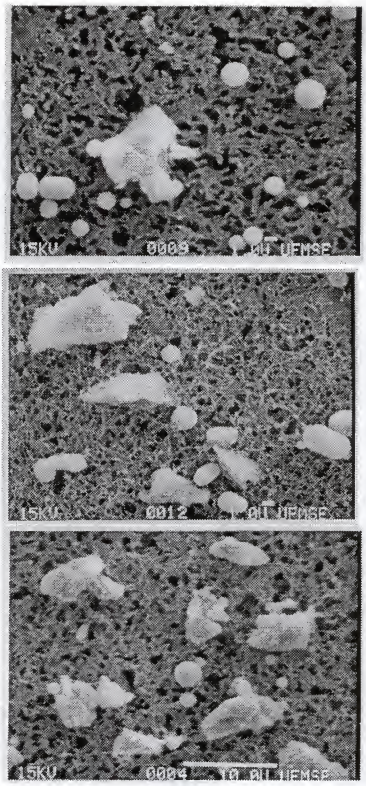


Figure 6-9. Higher magnification images of (a) glass, (b) macor and (c) soil particles. Note difference in scale for soil. (Bar represents 1 μm in (a) and (b); 10 μm in (c)).

A simple measurement was made to assess whether matrix effects, in terms of the composition of the ablation product, were significant between the glass, Macor®, and soil samples. In a stricter sense, matrix effects also refer to the differences in ablated mass. In this instance, only the representativeness of the ablation product was of interest, since the scattering signal could be used for mass correction with the glass and Macor® samples. Aluminum, which was a percent level constituent in each sample, was measured in addition to silicon for each matrix. The RSF's (Al/Si) obtained for the glass and Macor® were identical (RSF = 2.30), while soil produced a significantly different value (RSF = 3.40). This illustrated that matrix effects associated with the composition of the ablation product were not significant between the glass and Macor® ceramic, and provided further evidence of the utility of glasses for calibration of ceramic materials.

## Conclusions

The use of light scattering for LA-ICP-MS signal normalization was demonstrated for a variety of matrices. For measurements between matrices, it was important that the particle sizes generated by ablation were similar, as was demonstrated for glass, Macor®, and soil samples. The use of this technique was not as effective as the use of an internal standard in terms of the precision obtained. Light scatter normalization, however, requires no *a priori* knowledge of the sample heterogeneity or elemental composition. It provides a mass normalization alternative when a suitable internal standard is not available and its potential utility for the analysis of ceramic materials based on glass standard reference materials has been demonstrated.

# CHAPTER 7
# ANALYSIS OF SOIL AND SEDIMENT SAMPLES

## Introduction

The elemental analysis of soils is important for several reasons, with one of the most important being the identification of contaminants and establishment of levels of toxic elements present in the soil. The well-known toxic elements include arsenic, beryllium, cadmium, mercury, lead, antimony, tellurium, and thallium (7). In addition, many elements that are essential at low levels (e. g. cobalt, iron, zinc, and copper), become toxic at high levels (7). Therefore, sensitive and accurate techniques are required for the characterization of soil samples. An additional complicating factor in trace element toxicity is the symbiotic nature of coexisting metal species. For example, the presence of selenium has been shown to provide some protection against heavy metal toxic effects (7). This emphasizes the importance of multielement techniques for analyzing soil and other environmental samples.

The refractory nature of geological materials complicates the determination of elememental constituents in soils (7). Traditional methods of analysis rely on decomposition of the sample, typically through microwave digestion, and analysis of the resulting solution by flame or furnace atomic absorption spectrometry (AAS) or ICP-AES/MS. Direct methods of analysis are advantageous because of the elimination of time-consuming sample preparation steps and the risk of sample contamination from chemical

reagents. X-ray fluorescence is commonly used for the analysis of soils; however, the technique lacks the sensitivity to determine many low level species of interest.

Recently, laser sampling techniques have gained popularity for analyzing soil samples, since little to no sample preparation is required. Laser induced breakdown spectroscopy (LIBS) is well suited for field based analysis of soil samples, as evidenced by the number of recent publications on this application (6, 95, 96). The technique, however, suffers from more severe matrix-effects and poorer sensitivity when compared to LA-ICP-MS. Relatively few applications of LA-ICP-MS for analyzing soils have been reported (97-100). These applications have used either soil standards (97, 98, 100) or fused beads of soil (99) for analysis.

In this work, soil samples were analyzed by LA-ICP-MS and the utility of solution-based calibration was investigated. Sampling strategy and choice of the internal standard were found to be critical for obtaining accurate and precise results. Accuracy was reasonably good (+/- 20 %) for most elements studied; however in some cases, significant differences (around a factor of 3) were observed. To account for these discrepancies, several potential sources of error were investigated. These included speciation effects, organic content of the soil, and particle size effects. In addition, standard additions was studied for analyzing trace elements in soils. The effect of particle size on the utility of standard additions was studied.

## Experimental

The LA-ICP-MS instrumentation (Chapter 3) and operating conditions (Chapter 4) have been previously described. The laser was operated at 5 Hz with typical pulse energies of 0.7 mJ. Single spot sampling and translation sampling were both used in this

work and a comparison of the two will be made. Typical analysis times were 60 s (signals averaged over 300 laser shots).

The solution calibration methodology was discussed in Chapter 4. Several soil and sediment standard reference materials were analyzed to determine the applicability of solutions for calibration of these materials. These materials included NIST 2704 (Buffalo River Sediment), NIST 2709 (San Joaquin Soil), NIST 2710 (Montana Soil), NIST 2711 (Montana Soil), High Purity Standards (HPS) (Charleston, SC) Sandy Soil B, and High Purity Standards Loam A. The samples were pressed into pellets at a pressure of 35 MPa without any binder for analysis. A single multielement solution containing 2 ppm of Ca and 20 ppb of all other analytes was used to determine solution relative sensitivity factors (RSF's). RSF's were used, as discussed in Chapters 4 and 5, to determine analyte concentrations in the soils. Choice of an appropriate internal standard was found to be critical in the analysis of soil samples. This will be described more thoroughly in the experimental results.

To study the effect of organic content of the sample on LA-ICP-MS results, cellulose binder (Spex CertiPrep Metuchen, NJ) was added to NIST 2709 soil in varying proportions (10 % and 20 % w/w). The 1 g soil and binder samples were mixed in plastic vials with a Spex Mixer/Mill (Model 8000) for 30 minutes and then pressed into a pellet. Additionally, an inorganic sample (NIST 1633 Coal Fly Ash) was studied. With the coal fly ash standard, a sample mixed with cellulose binder (10 % w/w) was prepared, as well as one mixed with high-purity graphite (20 % w/w). The 1 g samples were pressed into pellets at 35 MPa.

Because elements exist in a variety of forms (e. g. carbonates, silicates, oxides, etc.) in soils, the effect of speciation on LA-ICP-MS results was studied. Samples containing various compounds of Ba were prepared in a sand matrix (Mallickrodt Baker, Inc. Paris, KY). Compounds of Ba (nitrate, oxide, chloride, carbonate, and sulfate) (Aldrich Chemical Company, Inc. Milwaukee, WI) were added to 10 g of sand to produce samples with a total Ba concentration of ~750 ppm. In addition, Ni (as sulfate) was added at the same concentration (~500 ppm) in each sample for use as an internal standard. Each of the mixtures was ground and homogenized in an alumina grinding vial (Spex Model 8003) for 30 minutes. A 0.9 g portion of the sample was then mixed with 0.1 g of cellulose binder for 30 minutes before being pressed into a pellet. To study the matrix dependence of speciation effects, Ba (and Ni as internal standard) samples were prepared in a graphite matrix. Direct grinding and mixing of the Ba and Ni compounds in graphite, however, did not produce homogeneous samples. It was necessary to prepare concentrated mixtures (10 % w/w) of Ba and Ni in sand, and then dilute this mixture in graphite to give final concentrations of ~750 ppm for both analytes.

To determine whether differences (composition, measurement precision, etc.) were observed for different particle size fractions, NIST 2704 and HPS Sandy Soil B samples were sieved into two different size fractions (<35 μm and 35 to 60 μm). One gram samples of each fraction were then pressed into pellets for analysis.

The utility of standard additions for accurate analysis of trace elements in soil was briefly assessed. Multiple standard additions of Co to NIST 2709, NIST 2710, and NIST 2711 were made by spiking the soil samples with Co solutions. The concentrations of the solutions were adjusted so that the same volume (3 mL) was added to 1 g soil samples.

The mixture was then dried at 110 °C for several hours in glass vials. Dried soil samples were then transferred to mixing vials and shaken for 10 minutes to ensure homogeneity. They were then pressed into pellets. To study the effect of particle size on standard addition measurements, sand samples of various particle sizes were spiked with a multielement solution. To generate a range of particle sizes, sand samples (~10 g) were ground for 1 to 2 minutes. The ground material was then transferred to the sieve and four particle size fractions (<35 μm, 35-60 μm, 60-80 μm, and >80 μm) were obtained. One gram samples of the different particle size fractions of sand were placed in glass vials, spiked with solutions containing Co, Ag, Y, Rb, W, Ba, and Pb, and dried at 110 °C for several hours. The sand samples were then mixed with 10 % (w/w) cellulose binder for 30 minutes and pressed into pellets for analysis.

## Results

### Spot Sampling Versus Line Sampling

Single spot and translational line sampling were studied for the analysis of soils. Signals were typically a factor of 4 or 5 larger when the sample was translated. This increase was greater than what was observed with glass and ceramic samples, most likely because a deep crater was formed more quickly in these compacted particulate samples. A comparison of the results obtained with both sampling strategies is shown in Figure 7-1 for NIST 2704. These figures represent the analyte responses for Ba and Ni relative to Ca from a total of 25 scans obtained from 25 different spots on the sample, or at different lines (5 scans/line) produced from translation of the sample. Cu and Co were also studied and produced similar results. The relative analyte responses from both sampling methods were similar in most cases; however, significant deviations from the mean (as much as a

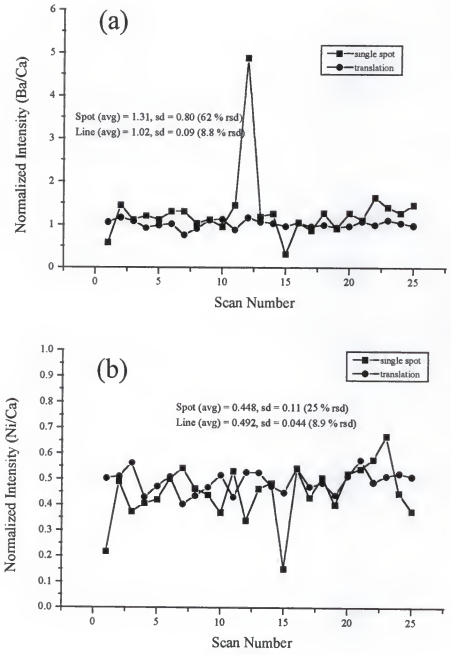


Figure 7-1. Comparison of relative analyte signals for (a) Ba and (b) Ni using both single spot and translational sampling.

factor of 5) were observed in some scans when sampling at a fixed location. This must have resulted from local inhomogeneity in the soil samples, and clearly indicated the need to sample a large enough portion of the soil to ensure accurate and precise measurements. Measurement of these local inhomogeneities is required for accurate measurement of the bulk composition; however, their presence can significantly affect the precision of analyses. From the results in Figure 7-1, it appeared that translation of the sample effectively averaged out the inhomogeneities during a typical 1 minute analysis, which should result in more precise measurements. The absence of large deviations in the relative analyte signal (analyte/Ca) was almost certainly due to the larger mass ablated with sample translation. The average precision (% rsd) of the relative intensities for the four analytes studied was 8.8 % with translation sampling and 37 % with single spot sampling. Since higher sensitivity and better precision were obtained with translation of the sample, this mode of sampling was used for all subsequent measurements.

Solution-Based Calibration

Solution-based calibration required selection of an appropriate internal standard with a known concentration in the sample. For the analysis of glass samples (Chapter 4), it was demonstrated that reasonably accurate results could be obtained whether a trace element (e. g. Sr) or major matrix constituent (e. g. Ca) was used as the internal standard. Because of greater inhomogeneity in the soil samples, measurement of a minor isotope of a major matrix consitituent (Ca) was used to provide an acceptable level of precision. Using an isotope of Ca ($^{43}$Ca or $^{44}$Ca), which was present at levels of 1-3 % in the soils studied, as the internal standard resulted in typical precision values (% rsd, n = 10) of less than 10 %. Precision values were not consistent among the soils analyzed. Measurements

on the NIST 2704 sample exhibited the poorest level of precision, with % rsd values consistently around 10-12 %. With the other soils, the precision was typically around 6-7 % rsd. Measurement precision is obviously dependent on the concentration of analyte in the sample and the amount of material ablated; however, this cannot explain the poorer precision observed with the NIST 2704 sample. This sample contained levels of trace elements and Ca that were similar to the other samples. In addition, a similar mass (~ 50 ng/shot) was ablated for all of the soils studied. The differences in precision that were observed might have been related to differences in the particle size distribution for the NIST 2704 sample compared to the other soils. The effects of particle size on measurement precision will be examined later in this chapter.

Selection of the internal standard was found to be an important factor in obtaining accurate results for soils. Initially, Ca was used as the internal standard because it was present at significant levels in all of the samples and possessed minor isotopes that could be measured with the multiplier detector. Calcium was used for the glass calibration studies and was found to provide accurate results for all elements studied. This was not the case with the soil samples. A comparison of the RSF's for several elements (V, Co, Ni, Cu, Zn, Sr, Ag, Ba, and Pb) in NIST 2709 and NIST 2704 soils using $^{43}Ca$ as the internal standard is given in Figure 7-2. These plots have been normalized to solution RSF values; therefore, the accuracy of the solution calibration method can be directly assessed by comparing the normalized soil RSF's to a value of one (a value of one signifies that solution and soil determined RSF's are identical). For NIST 2709, the measured concentrations of V, Co, Ni, Cu, and Zn were between 40 and 60 % higher than the certified values for these elements; Ba and Sr were about 60 % lower than the certified

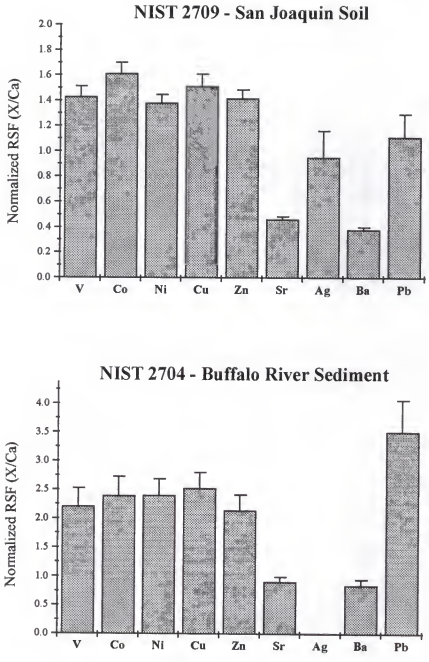


Figure 7-2. Comparison of RSF's for NIST 2709 and NIST 2704 soils. Plots have been normalized to solution RSF values.

values; and Pb was within 10 % of the certified value. For NIST 2704, different results were obtained. There was a systematic increase in the measured concentration for all of the analytes studied in this sample. Systematic changes were observed for the other soils as well. Because errors in the measured concentrations were largely systematic, rather than random, it is believed that they were the result of a spectroscopic interference by aluminum oxide at m/z 43. Based on these observations, $^{43}Ca$ was deemed a poor choice for internal standardization since the signal at this mass was affected by the levels of aluminum in the sample. The use of $^{44}Ca$ was also investigated for internal standardization. Similar systematic differences in the measurement accuracy were observed with this isotope as well, most likely as a result of interferences due to silicon oxide or carbon dioxide at m/z 44. Using an isotope of silicon ($^{28}Si$, $^{29}Si$, or $^{30}Si$) as the internal standard worked well for the analysis of minor elements in soil (Figure 7-3); however, none of the silicon isotopes could be measured on the multiplier detector due to saturation of the detector. Use of the multiplier was required for trace element analyses. Because of the interferences on Ca istopes and the lack of any other suitable internal standard that could be used over the whole series of soils, a minor sample constituent was used for further solution calibration work.

The use of trace elements as internal standards produced more accurate measurements for the soil samples. This is illustrated in Table 7-1, which compares the measured concentrations for several analytes in NIST 2704, NIST 2709, and NIST 2711 soils using the solution calibration method with both $^{43}Ca$ and $^{60}Ni$ as internal standards. The RSF values using Ni as the internal standard were determined by dividing the analyte/Ca RSF by the Ni/Ca RSF. Significantly more accurate results were obtained

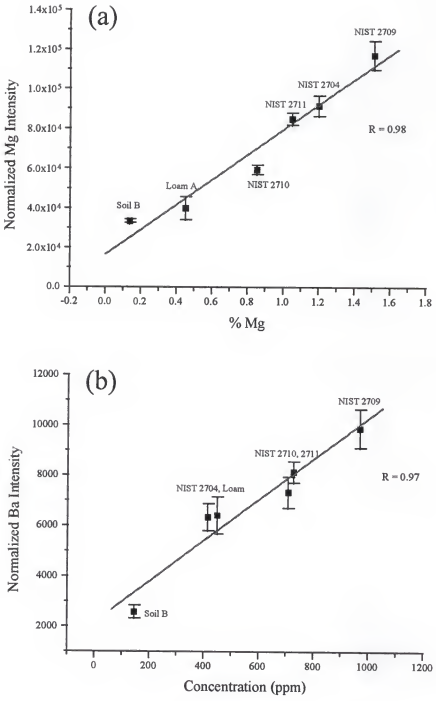


Figure 7-3. Calibration plots for (a) Mg and (b) Ba in soil samples using $^{28}Si$ as an internal standard.

Table 7-1. Measured concentrations in soils using solution calibration with $^{43}Ca$ and $^{60}Ni$ as internal standards.

| | NIST 2704 | | | NIST 2709 | | | NIST 2711 | | |
|---|---|---|---|---|---|---|---|---|---|
| | Cert. (ppm) | Meas.[a] $^{43}Ca$ (ppm) | Meas.[a] $^{60}Ni$ (ppm) | Cert. (ppm) | Meas.[a] $^{43}Ca$ (ppm) | Meas.[a] $^{60}Ni$ (ppm) | Cert. (ppm) | Meas.[a] $^{43}Ca$ (ppm) | Meas.[a] $^{60}Ni$ (ppm) |
| **V** | 95 | 210 ± 36 | 87 ± 15 | 112 | 160 ± 12 | 116 ± 10 | 81.6 | 106 ± 9 | 57.8 ± 4.7 |
| **Cr** | 135 | 326 ± 48 | 135 ± 22 | 130 | 146 ± 12 | 106 ± 11 | (47) | 59.8 ± 6.7 | 32.5 ± 4.8 |
| **Co** | 14.0 | 33.6 ± 5.2 | 13.9 ± 2.6 | 13.4 | 21.6 ± 1.3 | 15.6 ± 1.4 | (10) | 18.4 ± 2.3 | 9.2 ± 1.0 |
| **Ni** | 44.1 | int. std. | int. std. | 88 | int. std. | int. std. | 20.6 | int. std. | int. std. |
| **Cu** | 98.6 | 249 ± 31 | 103 ± 16 | 34.6 | 52.3 ± 3.9 | 37.9 ± 3.8 | 114 | 182 ± 18 | 110 ± 16 |
| **Zn** | 438 | 940 ± 140 | 390 ± 72 | 106 | 150 ± 9.3 | 109 ± 9 | 350.4 | 471 ± 56 | 255 ± 38 |
| **Sr** | (130) | 119 ± 12 | 49.0 ± 8.2 | 231 | 107 ± 5.3 | 77.5 ± 5.8 | 245.3 | 139 ± 9 | 75.6 ± 5.6 |
| **Ag** | | | | 0.41 | 0.39 ± .10 | .28 ± .08 | 4.63 | 7.2 ± 1.3 | 3.9 ± 0.8 |
| **Ba** | 414 | 351 ± 48 | 146 ± 34 | 968 | 369 ± 27 | 268 ± 23 | 726 | 439 ± 40 | 240 ± 30 |
| **Pb** | 161 | 570 ± 100 | 235 ± 58 | 18.9 | 21.1 4.2 | 15.3 ± 3.2 | 1162 | 3150 ± 210 | 1570 ± 140 |

[a] n = 5, 95 % confidence level

using Ni as the internal standard, thus indicating that solution calibration was useful even for a complex matrix like soil. A limitation of the technique, however, is that the concentration of some element that can serve as the internal standard must be known in the sample. This can be addressed by using a complementary technique to determine the concentration of an element in the sample, or by spiking in a known amount of some element that is not in the sample at an appreciable concentration relative to the amount added. A suitable element for spiking could be chosen by doing a survey scan over the sample of interest.

For the analytes studied, consistent patterns concerning the accuracy of solution calibration were observed. Most analytes (V, Cr, Mn, Co, Ni, Cu, and Zn) could be determined with reasonable accuracy (typically +/- 20 %) using a single solution for calibration; however, the measured concentrations for several analytes (Rb, Sr, Ba, and Y) were consistently lower (by around a factor of 2 or 3) than their certified values in the soils. More accurate measurements of the latter elements could be obtained if one element in this group was used as the internal standard for the other elements. The lower results obtained for Rb, Sr, Ba, and Y may be due to matrix effects resulting from high levels of efficiently ionized elements (EIE). EIE's generally cause a decrease in ICP-MS intensities, and are most severe for elements with low ionization energies (101). This might account for the lower results obtained for Rb, Sr, Ba, and Y, since these analytes possessed the lowest ionization energies of the elements studied. In general, matrix effects in ICP-MS are difficult to measure and quantify (23). They can often be minimized for particular analytes through optimization of the ICP-MS operating conditions or selection of appropriate internal standards (102); however, for multielement determinations, this is

often not feasible since all elements do not behave identically in the ICP-MS. Therefore, improvements with respect to one analyte may adversely affect the measurement of another analyte. The effect of ICP RF power on RSF's from solution and soil-based analytes was briefly studied to see if suitable conditions for analyzing Co, Cu, Sr, and Ba could be achieved. The results are presented in Figure 7-4. In these plots, Ni was used as the internal standard and all of the RSF values were normalized to the solution-based RSF value at 1200 W of RF power. Changing the RF power affected the RSF values slightly; however, the changes were similar for both the solution and the laser ablated NIST 2709 soil sample. Therefore, no improvement in the accuracy was observed as the RF power was changed over the range of 1050 to 1350 W.

Although accurate measurements were not obtained in all cases, solution calibration provided a relatively simple means of estimating analyte concentrations in the sample. In all cases, the measured analyte concentrations were within a factor of three of their certified concentrations, and in most cases, much better accuracy was achieved. To investigate potential sources of inaccuracy in soil samples, element speciation, sample organic content, and particle sizes effects were studied.

Speciation Effects

Since metals exist as a variety of compounds in soil samples, the effects of speciation on LA-ICP-MS measurements was examined. In a study involving the detection of Ba and Pb in soils by LIBS, it was determined that the chemical form (oxide, carbonate, sulfate, chloride, nitrate) of the analyte affected the sensitivity of LIBS measurements (6). To see if this might help explain the errors observed for Ba, Sr, Rb, and Y in this LA-ICP-MS work, the effects of speciation on Ba in a sand matrix was examined. The results for

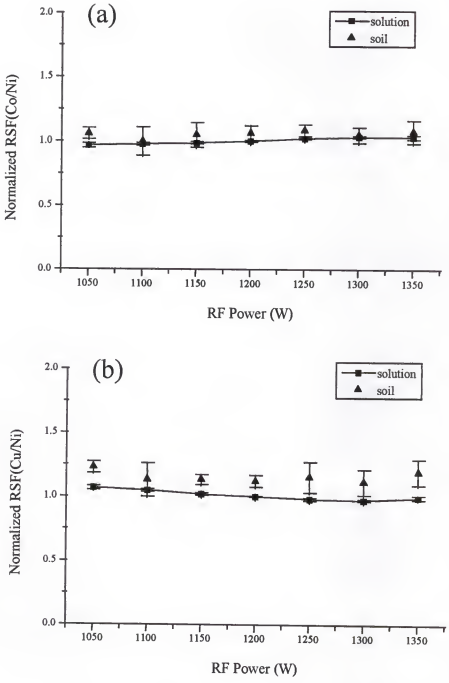


Figure 7-4. Effect of RF power on RSF's (solution and soil) for Co, Cu, Sr, Ba.

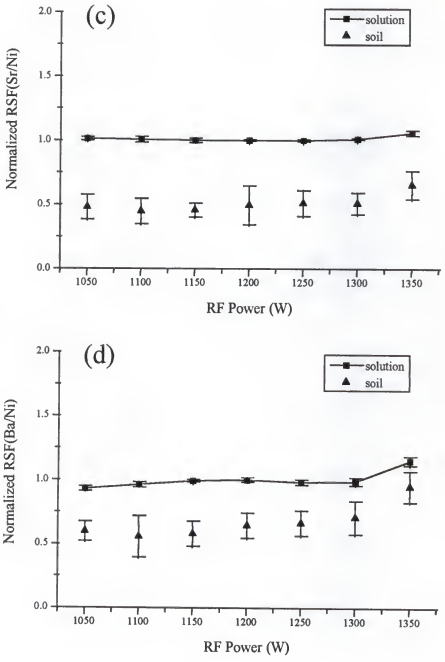


Figure 7-4 continued.

Table 7-2. Ba speciation results (sand matrix).

| | LA-ICP-MS RSF(Ba/Ni)[a,b] | LA-ICP-MS RSF($Ba_{total}$/Ni)[a,c] | ICP-MS RSF(Ba/Ni)[a,d] |
|---|---|---|---|
| **Oxide** | 0.89 ± 0.09 | 1.18 ± 0.10 | 1.66 ± 0.02 |
| **Nitrate** | 1.22 ± 0.16 | 1.64 ± 0.17 | 1.70 ± 0.02 |
| **Carbonate** | 1.14 ± 0.07 | 1.50 ± 0.09 | 1.68 ± 0.04 |
| **Chloride** | 1.33 ± 0.09 | 1.75 ± 0.09 | 1.56 ± 0.01 |
| **Sulfate** | 1.19 ± 0.05 | 1.58 ± 0.05 | |

[a] n = 5, 95 % confidence level.
[b] laser ablation results using $Ba^+$ signal only.
[c] laser ablation results using $Ba^+$, $Ba^{2+}$, and $BaO^+$ signals.
[d] solution results using $Ba^+$ signal only.

these studies are given in Table 7-2. The first column of data compares the RSF(Ba/Ni) values obtained from the five sand samples. The BaO sample produced a lower value (statistically significant at 95 % confidence level); however, the decrease was minor in comparison to the factor of 2-3 lower concentration measured with solution calibration. To see if the observed decrease could be attributed to the formation of $Ba^{2+}$ or $BaO^{+}$, the signals for these isotopes were included in determining RSF's (column 2 of Table 7-2). The same trend was observed; BaO produced slightly lower RSF's compared to the other chemical compounds. The RSF values given in the last column of Table 7-2 were measured from the sand pellets by solution nebulization to ensure that the samples contained the same levels of Ba and Ni. A 5 mg portion of each sand sample was diluted in 20 mL of 5 % $HNO_3$ and then heated to dissolve the Ba and Ni species. The solutions were analyzed and the results indicated that the pellets contained reproducible levels of Ba and Ni. The sulfate pellet was not included because $BaSO_4$ was insoluble in the dilute $HNO_3$ solution.

The effects of speciation were examined in a graphite matrix as well. Only the oxide, sulfate, and carbonate forms of Ba were studied, with Ni (sulfate) as the internal standard. No significant differences between the Ba/Ni RSF's were observed. The RSF(Ba/Ni) values were $1.45 \pm 0.19$ for the oxide, $1.48 \pm 0.25$ for the sulfate, and $1.54 \pm 0.27$ for the carbonate. Based on the speciation studies with Ba, it was determined that the form of the analyte did not significantly affect LA-ICP-MS measurements.

Effect of Organic Content

To determine whether organic content of the sample influenced LA-ICP-MS measurements, both soil and coal fly ash samples were studied. Organic content was

studied not only to determine if this might help explain the observed discrepancies for Ba, Sr, Rb, and Y, but also to determine if the addition of cellulose binder, used in pellet preparation, affected the accuracy of results. Previous studies using solution nebulization ICP-MS have indicated that the addition of small amounts of organic solvents can either increase or decrease analyte signals. Allain, et al. found that the addition of glycerol or methane significantly enhanced signals for some analytes (As, Au, Se, Te, and As), while other analytes were essentially unaffected (103). These workers attributed the signal enhancements with addition of carbon to a modification of ionization equilibrium over a limited energy range (9-11 eV). The ionization energy of carbon (11.2 eV) is slightly above this range. Longerich reported ICP-MS signal suppression for several elements when various organic solvents were added to a 1 % $HNO_3$ solution. (104). The loss in sensitivity could be recovered, however, when the nebulizer gas flow rate was reduced from the level corresponding to the maximum for a 1 % $HNO_3$ solution.

Results for the analysis of NIST 2709 soil, which contained 1.2 % carbon (organic and inorganic), with no binder added, 10 % cellulose binder added, and 20 % cellulose binder added were compared (Table 7-3). No significant changes in the measured analyte concentrations were observed with the addition of cellulose binder at levels up to 20 %. Similarly, a coal fly ash sample was studied to determine if different results were obtained when 10 % cellulose or 20 % graphite was used to prepare the sample pellet. The results for these analyses (Table 7-4) indicated that the addition of an inorganic (graphite) or organic (cellulose) binder produced similar results. The accuracy of these measurements, based on solution calibration with Ni (98 ppm in sample) as the internal standard, was around 10-20 % for all analytes studied.

Table 7-3. Comparison of RSF's from NIST 2709 soil with and without binder.

| | RSF[a] No cellulose | RSF[a] 10 % cellulose | RSF[a] 20 % cellulose |
|---|---|---|---|
| **V** | 32.8 ± 2.7 | 34.3 ± 1.0 | 36.2 ± 1.4 |
| **Cr** | 3.24 ± 0.30 | 3.45 ± 0.38 | 3.55 ± 0.26 |
| **Mn** | 35.6 ± 4.1 | 35.9 ± 1.9 | 36.3 ± 2.3 |
| **Co** | 36.5 ± 2.1 | 37.4 ± 1.0 | 40.4 ± 3.6 |
| **Ni** | 7.04 ± .36 | 7.01 ± 0.25 | 7.69 ± 0.50 |
| **Cu** | 16.4 ± 0.9 | 16.7 ± 0.8 | 18.6 ± 1.4 |
| **Zn** | 3.48 ± 0.17 | 3.51 ± 0.25 | 3.73 ± 0.33 |
| **Rb** | 11.6 ± 0.9 | 12.1 ± 0.69 | 14.0 ± 0.6 |
| **Y** | 16.7 ± 2.7 | 15.3 ± 1.4 | 16.6 ± 3.0 |
| **Ba** | 1.41 ± 0.16 | 1.40 ± 0.11 | 1.39 ± 0.08 |

[a] n = 5, 95 % confidence level. $^{43}Ca$ as internal standard.

Table 7-4. Measured concentrations from NIST 1633 (coal fly ash) with different binders using solution calibration.

| | Cert. Conc. (ppm) | Meas. Conc. (ppm)[a] 20 % graphite | Meas. Conc. (ppm)[a] 10 % cellulose |
|---|---|---|---|
| **V** | 214 ± 8 | 239 ± 12 | 244 ± 9 |
| **Cr** | 131 ± 2 | 153 ± 14 | 160 ± 8 |
| **Mn** | 493 ± 7 | 571 ± 21 | 579 ± 43 |
| **Cu** | 128 ± 5 | 143 ± 3 | 153 ± 10 |
| **Zn** | 210 ± 20 | 223 ± 9 | 235 ± 15 |
| **Cd** | 1.45 ± 0.06 | 1.65 ± 0.27 | 1.83 ± 0.26 |

[a] n = 5, 95 % confidence level. $^{60}Ni$ used as the internal standard.

Analysis of Particle Size Fractions

Two different particle size fractions of NIST 2704 and HPS Sandy Soil B were analyzed to determine whether analytes were distributed similarly in both fractions, and to determine how particle size affected the precision of LA-ICP-MS measurements when analyzing particulate samples. The results for NIST 2704 (Figure 7-5) indicated that the concentrations of the eight trace elements studied were identical, within the experimental uncertainty, in both particle size fractions. In these plots, the analyte response was normalized by $^{43}Ca$ to account for differences in ablated mass. The ablated mass was slightly higher (~20 %) for the pellet consisting of particles less than 35 μm, compared to the 35-60 μm pellet. Also, the precision of the measurements was significantly better for the smaller particle sample (average of 7. 3 % rsd) than the larger particle sample (average of 14 % rsd). The unsieved sample was included for comparison in Figure 7-5. The precision of measurements on this sample was intermediate of the two fractions, with an average % rsd of 10 %. The original material consisted of ~75-80 % of particles less than 35 μm.

The HPS Sandy Soil B sample produced different results in terms of particle composition. The Ca-normalized results (Figure 7-6) indicated that the smaller particles (<35 μm) had approximately three times more Pb and Ag than the larger particles (35-60 μm). All of the other elements studied contained identical levels of trace elements. These results are not easily explained, but might be related to the preparation of this standard reference material. In this soil, the concentrations of most trace elements have been enriched 10 to 100 times by spraying the sample with an aerosol mist. The samples were then dried, ground, sieved, and blended. If for instance, the elements were added

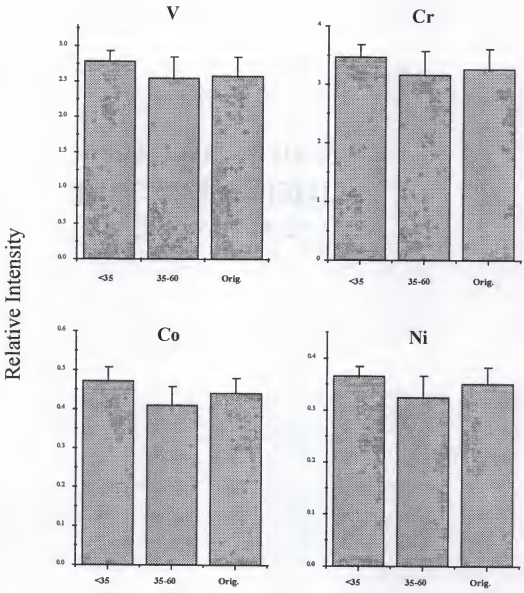


Figure 7-5. Comparison of relative analyte responses from different particle size fractions. Unsieved material included for comparison.

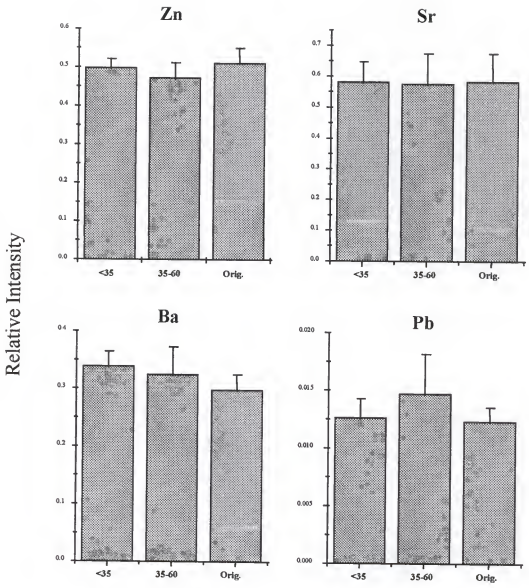


Figure 7-5 continued.

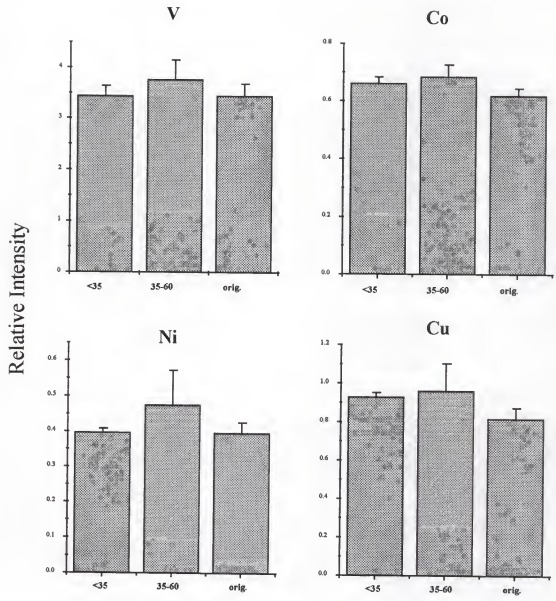


Figure 7-6. Comparison of relative analyte responses from different particle size fractions. Unsieved material included for comparison.

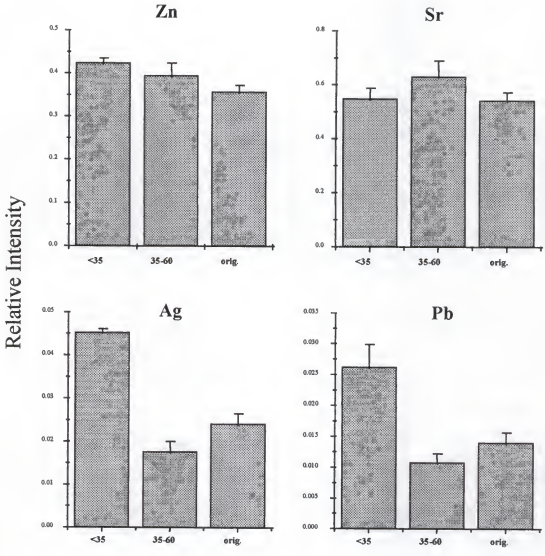


Figure 7-6 continued.

sequentially rather than simultaneously, a preferential adsorption of Pb and Ag on the smaller particles might have occurred. The behavior of these samples, in terms of measurement precision, was similar to that observed with the NIST 2704 sample. Measurements on the smaller particle sample were characterized by higher precision (average % rsd of 5.5 %) than the larger particle sample (average % rsd of 12 %). Precision of the measurements for the unsieved sample was 7.1 %, on average. Based on these studies, the precision of measuements is significantly affected by sample particle size. Samples consisting of larger particles produced poorer precision and lower ablation yields than samples consisting of smaller particles.

Analysis of Soils Using Standard Additions

Standard additions was briefly studied for analyzing Co in three soil samples (NIST 2709, NIST 2710, and NIST 2711). Although sample preparation time was increased with standard additions, standard additions possessed several advantages. Strict matrix-matching was achieved and the concentration of the internal standard was not required. This latter aspect is a limitation associated with the solution-calibration technique. With standard additions, an internal standard was still used to correct for variations in ablated mass. This was necessary to produce sufficiently precise measurements. In general, standard additions is well-suited for the analysis of soil and other particulate samples, since an element can be homogeneously spiked into the sample of interest. Results obtained for the analysis of Co in soils using multiple standard additions are given in Table 7-5. Only one of these materials was certified for Co (NIST 2709). The measured concentration of Co in this sample was not statistically different (95

Table 7-5. Results from the determination of Co in soils using multiple standard additions.

| | NIST 2709 | NIST 2710 | NIST 2710 |
|---|---|---|---|
| **Certified Conc. (ppm)** | 13.4 ± 0.7 | (10)[a] | (10)[a] |
| **Measured Conc. (ppm)** | 11.7 ± 1.6 | 8.5 ±0.8 | 7.5 ± 0.4 |

[a] non-certified value.

% level) than the certified value. Measured concentrations for the other samples were similar to the non-certified values.

In these measurements, the Co signal was normalized by the signal from a matrix element (Ca). To investigate whether particle size influenced relative signals for analytes deposited on the surface of particles to an analyte in the particle, several spiked sand samples were analyzed. The same amount of each analyte was added to four different size fractions of sand (<35 μm, 35-60 μm, 60-80 μm, and >80 μm). All analyte signals were normalized to $^{44}Ca$, which was present in the sand matrix. The results (Figure 7-6) indicated that the relative signals for all analytes increased significantly for particles greater than 35 μm. This was due to the inefficiency of the ablation process at the laser energies used (~0.5 mJ) in completely vaporizing the larger particles of sand. The deposited analytes were concentrated on the surface of the particles; therefore, they were preferentially vaporized relative to the bulk of the particle and produced higher relative intensities. Onset of this process should be shifted to larger particle diameters as the laser energy is increased; however, the energy used (0.5 mJ) was close to the maximum output of the laser system. In addition, particle sizes at which preferential vaporization became significant would depend on the type of sample being analyzed. For more refractory materials like ceramics, differences in relative analyte signals would be expected to occur at even smaller particle sizes. Based on the observed differences in relative analyte signals for the spiked sand samples, it was clear that particle sizes in the sample could significantly affect the accuracy of LA-ICP-MS results using the standard additions method. If the particles were too large to be efficiently ablated, only the surface concentration would be measured. For standard additions measurements, this would increase the slope of the

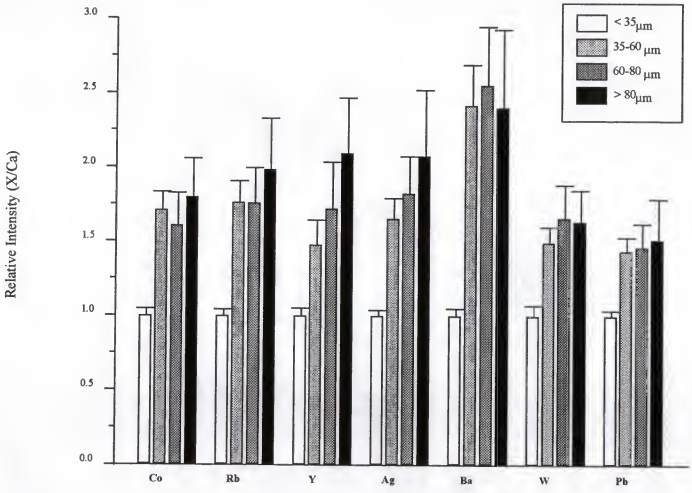


Figure 7-7. Effect of particle size on relative analyte signals for sand.

standard additions plot, and measured concentrations would be lower than what was actually present in the sample.

Detection limits

Detection limits (3σ) for elements in soil were typically in the tens of ppb range (Table 7-6), provided no major background interferences were present. This was demonstrated by the relatively poor detection limit for Cr (400 ppb), which resulted from interference by $ArC^+$.

## Conclusions

Reasonably accurate (+/- 20 %) results for most trace elements in soil samples could be obtained using a single solution standard. Poorer results were obtained for Rb, Sr, Y, and Ba, most likely because of matrix effects associated with large amounts of easily ionizable elements. Selection of an appropriate internal standard (e. g. Ni) was found to be important due to interferences on calcium isotopes. Elemental speciation and sample organic content did not significantly affect these measurements. Particle size was shown to play a significant role in terms of the precision of measurements. Measurements performed on samples that were composed of smaller particles were more precise. Standard additions was demonstrated to be useful for the analysis of Co in soil samples; however, studies indicated that particle sizes of the matrix could significantly affect the quality of these results, both in terms of accuracy and precision.

Table 7-6. Detection limits (3σ) for selected elements in soil.

| Analyte | Detection Limit (ppb) |
|---|---|
| V | 6 |
| Cr | 400 |
| Co | 3 |
| Ni | 30 |
| Cu | 20 |
| Zn | 200 |
| Sr | 8 |
| Ag | 4 |
| Cd | 30 |
| Ba | 30 |
| Pb | 200 |

# CHAPTER 8
# EVALUATION OF A COMPACT LASER SOURCE

## Introduction

The relative merits and applicability of laser sampling for ICP-MS have been previously discussed. In spite of the numerous advantages of the technique, the cost of commercially available laser ablation systems can be prohibitive. The most commonly used type of laser for LA-ICP-MS is the Nd:YAG operating at its fundamental wavelength (1064 nm) (19, 43, 71, 75-78) or one of its harmonics (532 nm (77-78), 355 nm (77), and 266 nm (66, 69, 70, 75-78)). Although it has been proposed that UV lasers may be more advantageous for LA-ICP-MS (76-78), the use of doubling crystals increases the complexity and expense of the system.

The purpose of this work is to report on the use of a compact and inexpensive Nd:YAG laser for LA-ICP-MS analysis of solids. These lasers, which were developed primarily for the ophthalmic market, offer a simple, low cost solid sampling option for ICP-MS users. The device, which measures approximately four inches in length, is permanently aligned and thus requires no manual adjustments (105). Recently, their use in a portable Laser Induced Breakdown Spectrometer was reported (95). In this work, the capability of these compact lasers for LA-ICP-MS analysis of NIST aluminum, copper, and glass samples is demonstrated.

## Experimental

The laser used in this study was a Nd:YAG (Kigre, Inc. Hilton Head, SC MK-367) operating at 1064 nm. This laser provided nominal pulse energies of 20 mJ, pulse widths of ~4 ns, and a beam diameter of around 3 mm. It could be powered from either a 12 V dc power source or a transformer for 110/120 V operation and had an operational lifetime in excess of 300,000 shots (105). It could be operated in either a manual firing mode or repetitively fired at a maximum repetition rate of 1 Hz. In our work, the laser was operated at 1 Hz, which required the use of a water-cooled mount (Kigre MK235236). The laser was focused onto the surface of the sample with a biconvex lens (6 cm focal length). Samples were held in a glass ablation chamber which was translated at ~50 μm/s on a modified syringe pump, to provide a partially fresh surface for each laser shot in order to achieve more representative sampling. The total cost of the laser system and sample stage was under $7000. Ablated material was transported to the ICP through a 1.5 m length of plastic tubing.

For comparison studies, the Finningan MAT System 266 laser ablation accessory (described in Chapter 3) was used. It provided a 266 nm Nd:YAG laser beam with a pulse energy of 0.5 mJ and a pulse width of 10 ns.

The ICP-MS instrumentation has been previously described (Chapter 3) Operating conditions were similar to those given in Table 4-1.

The samples used in this study included NIST 601-604 aluminum standard reference materials, in which titanium was present at levels of 120 to 1000 ppm. In the analysis of these samples, $^{48}Ti$ was measured as well as $^{57}Fe$ for internal standardization. In addition, NIST copper standard reference materials were analyzed for nickel ($^{60}Ni$

measured). The concentration of nickel in the samples ranged from 4.2 to 11.7 ppm. No internal standard was measured with the copper standards, since the only major matrix constituent (Cu) produced signals that were too large to measure with the multiplier detector. To minimize differences in ablated mass between these samples as a result of different laser focusing conditions, the samples were cut and polished to approximately the same height.

To demonstrate the utility of this laser for nonconducting samples, NIST glass samples were also analyzed (611, 612, and 617). In the glasses, $^{88}Sr$ and $^{43}Ca$ were measured, where Sr was present at levels from 41.5 ppm to 515.5 ppm and Ca was a major constituent of the glass matrix. All of these glasses were used as received with no surface modification or other preparation.

## Results

Scanning electron microscopy was used to examine the laser ablated NIST aluminum samples as shown in Figure 8-1. Figure 8-1a shows the surface of the sample after 50 laser shots. It can be seen that the largest amount of ablation occurs in a region approximately 150 μm in diameter, but that the melting of the sample extends well beyond this area as evidenced by the wavelike structures on the sample surface. Figure 8-1b is representative of typical analysis conditions, i.e., the sample was translated at 50 μm/s while the laser was fired at 1 Hz. The ablation track in this case is around 500 μm wide and very shallow. Once again, the wavelike structure can be clearly seen and is indicative of the fact that much of the material is removed by vaporization of the surface *via* the plasma that forms on the surface. For comparison, an ablation track formed by ablation with a 266 nm Nd:YAG is shown in 8-1c. It is evident from these figures that

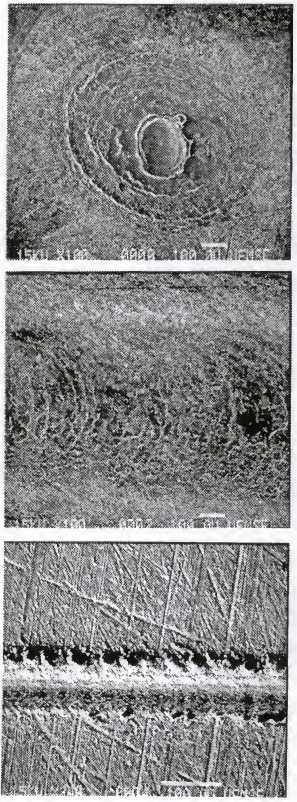


Figure 8-1. Scanning electron micrographs of aluminum surface after (a) 50 shots from the compact IR laser, (b) while translating the sample, and (c) with the UV laser while translating the sample. Magnifications of (b) and (c) are 100X and 240X, respectively. Bar represents 100 μm.

the ablation process is much more explosive with the UV laser than with the IR laser. This is due to the fact that the laser interacts with the sample surface throughout the laser pulse for UV lasers, and the role of the surface plasma in ablation is minimal. Several researchers have compared the use of IR and UV lasers for ablation (76-78). Only a limited comparison can be made in this work, however, since the pulse energy, pulse width, beam quality, and numerous other factors play a role in the ablation process.

A temporal profile of the Ti signal from NIST 604 is shown in Figure 8-2. This figure indicates that under the experimental conditions, even the low repetition rate of 1 Hz produced a "steady state" signal. The profile contains a large number of spikes, which can be attributed to larger particles being vaporized in the ICP.

A linear calibration plot ($R = 0.99$) was obtained for Ti in the aluminum samples (Figure 8-3). It was necessary with these samples to measure $^{57}Fe$ in addition to $^{48}Ti$, in order to account for differences in the mass ablated between samples and within a series of analyses on one sample. Although it is not exactly an internal standard since its concentration varied between the samples, we accounted for these differences by normalizing the signal and thus mimicked the use of an internal standard. It is usually preferable to use a minor isotope of a major matrix constituent as the internal standard, but this was not possible because Al is monoisotopic and produced signal levels that saturated the detector. The precision of the normalized measurements ($n = 5$) ranged from 10 to 13 % rsd, compared to 17 to 24 % without normalization. These values could be improved by using a shorter dwell time and a larger number of passes, but a minimum dwell time of 64 ms was required with the Faraday detector. This means that a relatively

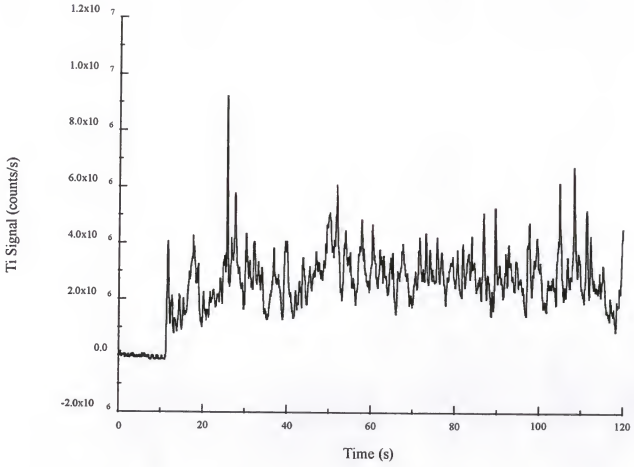


Figure 8-2. Temporal profile of Ti signal from NIST 604 aluminum.

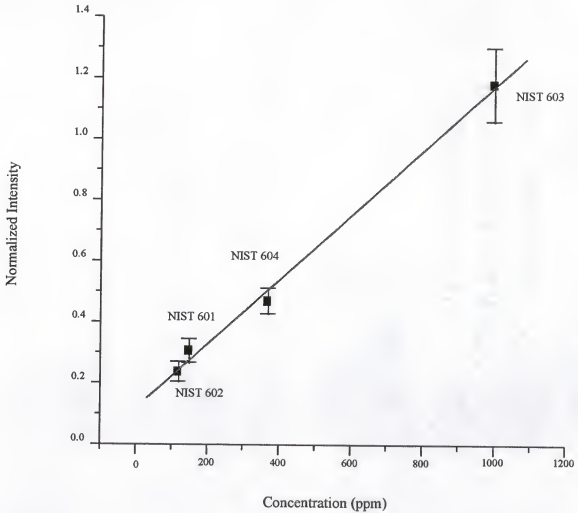


Figure 8-3. Calibration plot for Ti in aluminum samples.

long period of time was spent at each mass. The detection limit (3σ) for Ti in the aluminum samples was 0.3 ppm.

A linear calibration plot (R = 0.98) was also obtained for Ni in the NIST copper standard reference materials (Figure 8-4). Precision of these measurements, however, was relatively poor since no internal standard was used. The % rsd (n = 5) ranged from 12 to 39 %. The detection limit (3σ) for Ni was 0.02 ppm.

To assess the use of the laser for nonconducting samples, NIST glasses were analyzed. A linear calibration plot (R = 0.999) for Sr was obtained (Figure 8-5). As with the aluminum standards, an additional isotope ($^{43}Ca$) was measured to account for differences in the ablated mass. Differences in the ablated mass were as great as a factor of four between the glasses. This most likely resulted from differences in the 1064 nm absorption by the glass samples. Variations in the ablated mass between samples was less than a factor of two with the 266 nm laser, since essentially all the light was absorbed at this wavelength. The precision of the measurements (n = 5) ranged from 2 to 10 % rsd. The improved precision of these measurements, compared to the Ti in aluminum measurements, was at least partially due to the shorter dwell times that could be used with the multiplier detector. The detection limit (3σ) for Sr in the NIST glasses was 0.1 ppm. For comparison, the detection limit with UV laser ablation was 0.05 ppm. The improvement can be attributed to the larger mass of material that was ablated with the UV laser, due to increased absorption by the glass. Due to differences in laser ablation systems and ICP-MS instrumentation, direct comparisons with other researchers are difficult. Hager and coworkers reported a detection limit of 0.006 ppm for Sr in a glass matrix, but their work was performed with an IR laser with much higher energy

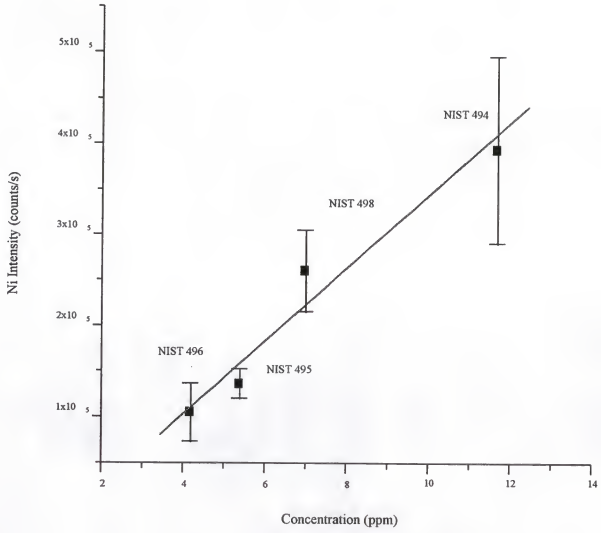


Figure 8-4. Calibration plot for Ni in copper samples.

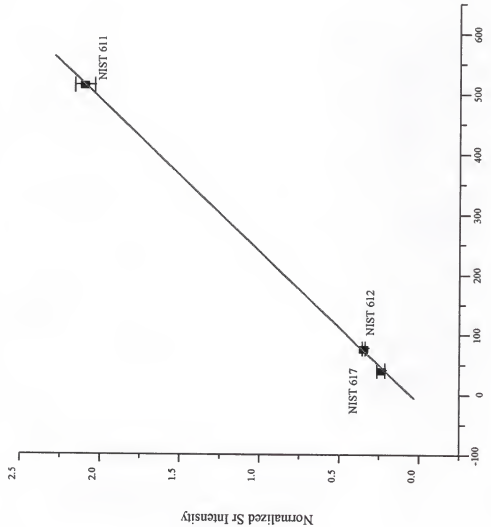


Figure 8-5. Calibration plot for Sr in glass samples.

(hundreds of millijoules) and a higher repetition rate (10 Hz) (12). This would result in much larger quantities being introduced to the ICP-MS and therefore, at least partially, explains the much lower detection limit. In addition, it is not clear whether single ion monitoring was used (as opposed to multielement scanning) in determining the detection limit, as this can result in significant improvements in detection limits.

## Conclusions

The results obtained with the compact laser system indicate that it can be successfully coupled with an ICP-MS to achieve sub-ppm detection limits for analytes in both conducting and nonconducting matrices. Detection limits for Sr in the NIST glasses are a factor of two higher than those obtained with the commercially available UV laser system. In addition, spatial resolution is not as good for IR lasers compared to UV lasers. This is due to diffraction limitations, as well as differences in laser sampling mechanisms for IR and UV lasers (laser-material, laser-plasma, and plasma-material interactions). For bulk sampling of solids, however, the compact Nd:YAG provides a potentially useful, simple, and relatively inexpensive option for ICP-MS users.

# CHAPTER 9
# CONCLUSIONS AND FUTURE WORK

## Conclusions

Laser ablation inductively coupled plasma mass spectrometry (LA-ICP-MS) has been used to analyze a variety of materials. The technique has a number of advantages, most notable is the ability to directly analyze essentially any solid material with little or no sample preparation. It is a sensitive (sub-ppm detection limits) multielement technique that can be used for both bulk and low-resolution (μm scale) spatial analysis. As with most other solids techniques, the major limitation to the widespread applicability of LA-ICP-MS is the existence of matrix effects. The matrix effects are relatively minor, however, and semiquantitative work is easily performed. For quantitative analysis, matrix-matched standards are usually required. Unfortunately for some materials, standards do not exist and alternative calibration approaches must be sought.

In this work, the use of solutions for calibration of solid materials was studied. It was demonstrated that reasonably accurate results (± 20 % typically) could be obtained from a range of samples (glass, ceramic, soil, and coal fly ash), provided that proper ablation and ICP-MS conditions were chosen. An additional benefit of using the "wet plasma" configuration associated with dual sample introduction was that it provided higher sensitivity and better precision. The importance of laser irradiance and sampling strategy on representative sampling was demonstrated for glasses. The laser irradiance

should exceed $2x10^8$ W/cm$^2$ to avoid fractionation of elements during the ablation process. Sampling strategy (stationary of translated sample) was an important consideration for all analyses. Translation of the sample resulted in larger ablation rates; however, the sampling depth was considerably smaller than depths produced without translation. The sample heterogeneity dictated which sampling strategy was most suitable for a particular material.

Solution calibration was extended to the analysis of ceramics. Silicon nitride ceramic bearings were analyzed and the results for minor elements obtained with the solution calibration approach were confirmed by X-ray microanalysis. In addition, glass standard reference materials were demonstrated to be useful for the analysis of silicon nitride ceramics, provided the difference in ablated mass between the samples was accounted for. This led to an investigation of light scattering for mass normalization.

Mass normalization based on light scattering was useful. It effectively corrected for differences in ablated mass between a glass and a ceramic material, as a consequence of similar-sized ablated particulates from these materials. This meant that absolute sensitivity values determined from a standard glass material, rather than relative sensitivity factors, could be used for analyzing ceramics. In other words, the concentration of an element in the sample of interest (internal standard) was not required. Use of an internal standard of known concentration was required with solution calibration. An internal standard was also used when calibrating with solids, since the ablated mass typically varied from sample to sample. Using light scattering eliminated restrictions associated with internal standardization, such as the requirement that the

analyte and internal standard be distributed similarly in the solid. Light scattering might be most useful for analyzing inhomogeneous or multilayered samples.

The analysis of soils presented several challenges that were unique to this matrix. The importance of selecting an appropriate internal standard was demonstrated for the analysis of soils using solution calibration. Interferences on Ca isotopes prevented their use as internal standards for quantitative work; therefore, a trace element (Ni) was used to demonstrate the utility of solution calibration. An internal standard that behaved similar to the analyte with regards to ICP-MS matrix effects was required. This was important for the analysis of Sr, Y, Rb, and Ba in soil, since the relative signals for these analytes were suppressed when compared to aqueous solutions. The effect of element speciation on LA-ICP-MS signals was studied, and it was demonstrated that signals were largely unaffected by the anionic constituent of the analyte. In addition, the level of organic material in the sample had no appreciable affect on LA-ICP-MS results. For pressed particulate samples, particle size of the matrix constituents significantly influenced the precision of measurements. Precision improved as the particle size was reduced. Particle size was demonstrated to be an important consideration with standard additions measurements as well, since relative analyte signals for spiked sand samples increased when the particle size exceeded 35 μm.

Finally, a compact Nd:YAG laser was evaluated for the analysis of glass and metal samples. It was demonstrated that the laser might be useful for bulk analysis of solids, since it was inexpensive, easily set-up, and provided sub ppm detection limits for analytes in a variety of matrices.

## Future Work

This research has opened up a range of future investigations. Light scatter normalization should be refined and extended to determine the full extent of its capabilities. The influence of scatter collection angle on the effectiveness of normalization within and between matrices should be investigated. In addition, the work should be extended to applications where normal internal standardization cannot be used, such as with multilayered ceramics or inhomogeneous geological samples. In these cases, analyte signals could be measured with the ICP-MS and the light scatter signal could be used for mass correction. Therefore, the concentration of the analyte throughout the sample could be reliably determined. This would not be possible with internal standardization, since no element would be present throughout the sample at identical levels. Light scattering, however, does depend on the physical properties (refractive index, particle size, etc.) of the ablated material, and the scatter signal-mass signal relationship will have to be explored more thoroughly.

The spatial and depth profiling capabilities of the LA-ICP-MS system need to be examined. Single shot ablation removes sub-μm layers from the sample surface, therefore, the analysis of μm layers of coatings is possible. Additionally, LA can be used to analyze relatively thick layers (hundreds of microns), which cannot be done with other surface analysis techniques. Application of LA-ICP-AES to the analysis of thick layers of coating has recently been reported (16); however, the use of LA-ICP-MS could be advantageous if high sensitivity is required. The in-depth resolution of laser sampling is determined by the rate at which material is removed from the surface; therefore, low repetition rates and/or translation of the sample should be employed. Low repetition rates

can be problematic, however, because transient signals are generated. With a scanning instrument, this makes mass normalization difficult, since the signal is changing rapidly in comparison to the time spent at each mass location. If light scatter normalization is used, the scattering signal that is produced from a single pulse can be used for mass correction. Light scatter normalization based on single shot measurements has not been examined in this work, however, scattering signals have been obtained for single shots on glass samples.

Additional work could be performed with soil and particulate samples. The lower relative sensitivities for Sr, Rb, Y, and Ba were explained on the basis of high levels of easily ionizable elements (EIE). The EIE effect could be studied by spiking these analytes, as well as several others analytes for which no suppression was observed, into several different matrices, such as graphite and sand. To these matrices, increasing levels of an EIE (e. g. Na) could be added to determine if the EIE affected relative analyte signals. Also, more extensive studies on ICP-MS operating conditions would be useful to determine if suitable conditions could be obtained for the analysis of all analytes in soil. In a study involving solution nebulization ICP-MS of dissolved steel samples, it was demonstrated that nebulizer flow rate significantly influenced the extent of matrix effects (102). By decreasing the nebulizer flow rate, matrix effects were reduced, although with a loss in sensitivity. Similarly, the influence of flow conditions on matrix effects in LA-ICP-MS analyses could be studied.

Additionally, the combined use of standard additions and solution calibration could be explored. As mentioned, the major limitation of solution calibration was that the concentration of the internal standard was required. For the analysis of glass and

ceramics, this limitation could be overcome by measuring light scattered from the ablation product. For soil and particulate samples, an internal standard of known concentration could be spiked directly into the sample. A brief survey scan of the sample of interest could be used to identify elements that did not exist at appreciable levels in the sample. This element could then be spiked into the sample, to serve as the internal standard. As demonstrated in Chapter 7, the applicability of spiked samples for calibration would depend on the type and size of particles present in the sample. The use of internal standards could be studied for a wide range of materials (soils, ceramics powders, etc.) and analytes to determine the limitations of this approach.

## REFERENCES


1. M. Franek, V. Krivan, B. Gercken, and J. Pavel, Mikrochim. Acta **113**, 251 (1994).

2. B. Gercken, J. Pavel, and O. Suter, in *Applications of Plasma Source Mass Spectrometry II*, G. Holland and A. N. Eaton, Eds. (The Royal Society of Chemistry, Thomas Graham House, Cambridge, 1993).

3. V. Balaram, Current Sci. **69**, 640 (1995).

4. K. H. Wedepohl, Ed. *Handbook of Geochemistry*, Vol. I-II (Springer-Verlag, New York, 1970).

5. G. Zaray and T. Kantor, Spectrochim. Acta **50B**, 489 (1995).

6. A. S. Eppler, D. A. Cremers, D. D. Hickmott, M. J. Ferris, and A. C. Koskelo, Appl. Spectrosc. **50**, 1175 (1996).

7. J. C. Van Loon, *Selected Methods of Trace Metal Analysis: Biological and Environmental Samples* (John Wiley and Sons, New York, 1985).

8. R. Jenkins, *X-Ray Fluorescence Spectrometry* (John Wiley and Sons, New York, 1988).

9. J. I. Goldstein, D. E. Newbury, P. Echlin, D. C. Joy, A. D. Romig, Jr., C. E. Lyman, C. Fiori, and E. Lifshin, *Scanning Electron Microscopy and X-Ray Microanalysis* (Plenum Press, New York, 1994).

10. A. Lodding, in *Inorganic Mass Spectrometry*, F. Adams, R. Gijbels, and R. Van Grieken, Eds. (John Wiley and Sons, New York, 1988).

11. W. W. Harrison, in *Inorganic Mass Spectrometry*, F. Adams, R. Gijbels, and R. Van Grieken, Eds. (John Wiley and Sons, New York, 1988).

12. E. R. Denoyer, K. J. Fredeen, and J. W. Hager, Anal. Chem. **63**, 445A (1991).

13. D. M. Hercules and S. H. Hercules, J. Chem Ed. **61**, 592 (1984).

14. D. Milton and J. C. Hutton, Spectrochim. Acta **48B**, 39 (1993).

15. R. K. Marcus, J. Anal. At. Spectrom. **11**, 821 (1996).

16. V. Kanicky, I. Novotny, J. Musil, and J. -M. Mermet, Appl. Spectrosc. **51**, 1042 (1997).

17. S. A. Darke and J. F. Tyson, J. Anal. At. Spectrom. **8**, 145 (1993).

18. R. E. Russo, Appl. Spectrosc. **49**, 14A (1995).

19. A. A. van Heuzen, Spectrochim. Acta **46B**, 1803 (1991).

20. W. T. Perkins, R. Fuge, and N. J. G. Pearce, J. Anal. At. Spectrom. **6**, 445 (1991).

21. A. A. van Heuzen and J. B. W. Morsink, Spectrochim. Acta **46B**, 1819 (1991).

22. *Inductively Coupled Plasmas in Analytical Atomic Spectrometry, Second Edition*, A. Montaser and D. W. Golightly, Eds. (VCH Publishers, New York, 1992).

23. *Handbook of Inductively Coupled Plasma Mass Spectrometry*, K. E. Jarvis, A. L. Gray, and R. S. Houk, Eds. (Chapman and Hall, New York, 1992).

24. D. W. Douglas, Prog. Analyt. Atom. Spectrosc. **8**, 1 (1995).

25. R. S. Houk, Anal. Chem. **58**, 97A (1986).

26. J. W. Olesik, Anal. Chem. **63**, 12A (1991).

27. M. W. Blades and D. G. Weir, Spectroscopy, **9**, 14 (1994).

28. D. J. Douglas and J. B. French, J. Anal. At. Spectrom. **3**, 743 (1988).

29. *SOLA ICP/GD Mass Spectrometer Operators Manual*; Finnigan MAT Ltd. San Jose, 1993.

30. F. Vanhaecke, L. Moens, R. Dams, I. Papadakis, and P. Taylor, Anal. Chem. **69**, 268 (1997).

31. P. P. Mahoney, S. J. Ray, and G. M. Hieftje, Appl. Spectrosc. **8**, 16A, (1997).

32. D. W. Koppenaal, C. J. Barinaga, and M. R. Smith, J. Anal. At. Spectrom. **9**, 1053 (1994).

33. R. C. Hutton and A. N. Eaton, J. Anal. At. Spectrom. **2**, 595 (1987).

34. D. G. Weir and M. W. Blades, Spectrochim. Acta **45B**, 615 (1990).

35. J. W. McLaren, J. W. Lam, and A. Gustavsson, Spectrochim. Acta **45B**, 1091 (1990).

36. R. Tsukahara and M. Kubota, Spectrochim. Acta **45B**, 581 (1990).

37. A. L. Gray, Analyst **110**, 551 (1985).

38. M. Thompson, S. Chenery, and L. Brett, J. Anal. Atom. Spectrom. **4**, 11 (1989).

39. V. V. Kogan, M. W. Hinds, and G. I. Ramendik, Spectrochim. Acta **49B**, 333 (1994).

40. J. L. Imbert and P. Telouk, Mikrochim. Acta **110**, 151 (1990).

41. J. S. Becker, U. Breuer, J. Westheide, A. I. Saprykin, H. Holzbrecher, H. Nickel, and H. -J. Dietze, Fres. J. Anal. Chem. **355**, 626 (1996).

42. I. D. Abell, D. Gregson, and S. Shuttleworth, in *The Physics and Chemistry of Carbides, Nitrides, and Borides*, R. Freer, Ed. (Kluwer Academic Publishers, Dordrecht, The Netherlands, 1990).

43. F. E. Lichte, Anal. Chem. **67**, 2479 (1995).

44. A. M. Ghazi, T. E. McCandless, D. A. Vanko, and J. Ruiz, J. Anal. At. Spectrom. **11**, 667 (1996).

45. P. M. Outridge and R. D. Evans, J. Anal. At. Spectrom. **10**, 595 (1995).

46. J. Marshall, F. Franks, I. Abell, and C. Tye, J. Anal. At. Spectrom. **6**, 145 (1991).

47. N. Bloembergen, in *Laser Solid Interactions and Laser Processing*, S. D. Ferris, H. J. Leamy, and J. M. Poate, Eds. (American Institute of Physics, New York, 1979).

48. J. F. Ready, *Effect of High-Powered Laser Radiation* (Academic Press, New York, 1971).

49. R. Wisbrun, I. Schechter, R. Niessner, H. Schröder, and K. L. Kompa, Anal. Chem. **66**, 2964 (1994).

50. F. Hillenkamp, M. Karas, R. Beavis, and B. Chait, Anal. Chem. **63**, 1193A (1991).

51. W. Sdorra, A. Quentmeier, and K. Niemax, Mikrochim. Acta **II**, 185 (1989).

52. T. Kantor, L. Bezur, E. Pungor, and P. Fodor, Spectrochim. Acta **34B**, 341 (1979).

53. R. Wennrich and K. Dittrich, Spectrochim. Acta **42B**, 995 (1987).

54. Y. Iida, Spectrochim. Acta **45B**, 427 (1990).

55. A. Ciocan, L. Hiddemann, J. Uebbing, and K. Niemax, J. Anal. At. Spectrom. **8**, 273 (1993).

56. Y. Q. Tang and C. Trassy, Spectrochim. Acta **41B**, 143 (1986).

57. S. E. Long and R. F. Browner, Spectrochim. Acta **43B**, 1461 (1988).

58. C. N. Davies, *Aerosol Science* (Academic Press, New York, 1966).

59. P. Arrowsmith and S. K. Hughes, Appl. Spectrosc. **42**, 1231 (1988).

60. L. Ebdon, M. E. Foulkes, and S. Hill, J. Anal. At. Spectrom. **5**, 67 (1990).

61. K. E. Jarvis and J. G. Williams, Chem. Geol. **77**, 53 (1989).

62. R. J. Watling, B. F. Lynch, and D. Herring, J. Anal. At. Spectrom. **12**, 195 (1997).

63. A. Moissette, T. J. Shepherd, and S. R. Chenery, J. Anal. At. Spectrom. **11**, 177 (1996).

64. J. Stix, G. Gauthier, and J. N. Ludden, Can. Mineral. **33**, 435 (1995).

65. Z. Chen, W. Doherty, and D. C. Gregoire, J. Anal. At. Spectrom. **12**, 653 (1997).

66. B. J. Fryer, S. E. Jackson, and H. P. Longerich, Can. Mineral. **33**, 303 (1995).

67. L. Moenke-Blankenburg, T. Schumann, D. Günther, H. -M. Kuss, and M. Paul, J. Anal. At. Spectrom. 7, 251 (1992).

68. M. Ducreux-Zappa and J. -M. Mermet, Spectrochim. Acta **51B**, 321 (1996).

69. E. F. Cromwell and P. Arrowsmith, Anal. Chem. **67**, 131 (1995).

70. S. Chenery and J. M. Cook, J. Anal. At. Spectrom. **8**, 299 (1993).

71. J. W. Hager, Anal. Chem. **61**, 1243 (1989).

72. E. F. Cromwell and P. Arrowsmith, Appl. Spectrosc. **49**, 1652 (1995).

73. H. P. Longerich, D. Günther, and S. E. Jackson, Fres. J. Anal. Chem. **355**, 538 (1996).

74. X. Mao, W. -T. Chan, M. Caetano, M. A. Shannon, and R. E. Russo, Appl. Surface Sci. **96-98**, 126 (1996).

75. P. M. Outridge, W. Doherty, and D. C. Gregoire, Spectrochim. Acta **51B**, 1451 (1996).

76. T. E. Jeffries, N. J. G. Pearce, W. T. Perkins, and A. Raith, Anal. Comm. **33**, 35 (1996).

77. C. Geertsen, A. Briand, F. Chartier, J. -L. Lacour, P. Mauchien, S. Sjöström, and J. -M. Mermet, J. Anal. At. Spectrom. **9**, 17 (1994).

78. D. Figg and M. S. Kahr, Appl. Spectrosc. **51**, 1185 (1997).

79. *CRC Handbook of Chemistry and Physics*, D. R. Lide, Ed. (CRC Press, Boca Raton, 1994).

80. J. F. Chudecki, Ceramic Bulletin **69**, 1113 (1990).

81. J. A. C. Broekaert and G. Tölg, Mikrochim. Acta **II**, 173 (1990).

82. J. A. C. Broekaert, T. Graule, H. Jenett, G. Tölg, and P. Tschöpel, Fres. J. Anal. Chem. **332**, 825 (1989).

83. L. K. L. Falk and E. U. Engström, J. Am. Ceram. Soc. **74**, 2286 (1991).

84. C. Ziegler, J. Heinrich, and G. Wötting, J. Mat. Sci. **22**, 3041 (1987).

85. E. H. Homeier, S. A. Bradley, and K. R. Karasek, J. Mat. Sci. **27**, 1231 (1992).

86. J. S. Crighton, J. Carroll, B. Fairman, J. Haines, and M. Hinds, J. Anal. At. Spectrom. **11**, 461R (1996).

87. J. T. Westheide, J. S. Becker, R. Jäger, H. –J. Dietze, and J. A. C. Broekaert, J. Anal. At. Spectrom. **11**, 661 (1996).

88. P. Arrowsmith, in *Ceramic Transactions Vol. 5*, W. S. Young, G. L. McVay, and G. Pike, Eds. (American Ceramic Society, Westerville, OH, 1988).

89. H. Pang, D. R. Wiederin, R. S. Houk, and E. S. Yeung, Anal. Chem. **63**, 390 (1991).

90. T. Tanaka, K. Yamamoto, T. Nomizu, and H. Kawaguchi, Anal. Sci. **11**, 967 (1995).

91. P. Richner, M. W. Borer, K. R. Brushwyler, and G. M. Hieftje, Appl Spectrosc. **44**, 1290 (1990).

92. M. Ducreux-Zappa and J. –M. Mermet, Spectrochim. Acta **51B**, 333 (1996).

93. M. Thompson, S. Chenery, and L. Brett, J. Anal. At. Spectrom. **5**, 49 (1990).

94. Y. Huang, Y. Shibata, and M. Morita, Anal. Chem. **65**, 2999 (1993).

95. K. Y. Yamamoto, D. A. Cremers, M. J. Ferris, and L. E. Foster, Appl. Spectrosc. **50**, 222 (1996).

96. R. Barbini, F. Colao, R. Fantoni, A. Palucci, H. J. L. van der Steen, and M. Angelone, Appl. Phys. B **65**, 101 (1997).

97. S. F. Durrant and N. I. Ward, Fres. J. Anal. Chem. **345**, 512 (1993).

98. L. Moenke-Blankenburg, T. Schumann, and J. Nölte, J. Anal. At. Spectrom. **9**, 1059 (1994).

99. X. Guo and F. E. Lichte, Analyst **120**, 2707 (1995).

100. E. Hoffmann, C. Lüdke, and H. Stephanowitz, Fres. J. Anal. Chem. **355**, 900 (1996).

101. J. W. Olesik, Anal. Chem. **68**, 469A (1996).

102. M. –A. Vaughan and G. Horlick, J. Anal. At. Spectrom. **4**, 45 (1989).

103. P. Allain, L. Jaunault, Y. Mauras, J. –M. Mermet, and T. Delaporte, Anal. Chem. **63**, 1497 (1991).

104. H. P. Longerich, J. Anal. At. Spectrom. **4**, 665 (1989).

105. Kigre, Inc. 100 Marshland Road, Hilton Head Island, SC 29926.

## BIOGRAPHICAL SKETCH

Scott A. Baker was born in Pensacola, Florida, on June 10, 1971. He grew up in Charleston, South Carolina, and graduated from James Island High School in 1989. He received his Bachelor of Science degree in chemistry in May 1993 from the College of Charleston. He started graduate school at the University of Florida in August 1993, where he joined Dr. James D. Winefordner's research group. He received his Doctor of Philosophy in analytical chemistry in May 1998.

I certify that I have read this study and that in my opinion it conforms to acceptable standards of scholarly presentation and is fully adequate, in scope and quality, as a dissertation for the degree of Doctor of Philosophy.

James D. Winefordner, Chairman
Graduate Research Professor of Chemistry

I certify that I have read this study and that in my opinion it conforms to acceptable standards of scholarly presentation and is fully adequate, in scope and quality, as a dissertation for the degree of Doctor of Philosophy.

Willard W. Harrison
Professor of Chemistry

I certify that I have read this study and that in my opinion it conforms to acceptable standards of scholarly presentation and is fully adequate, in scope and quality, as a dissertation for the degree of Doctor of Philosophy.

Robert T. Kennedy
Associate Professor of Chemistry

I certify that I have read this study and that in my opinion it conforms to acceptable standards of scholarly presentation and is fully adequate, in scope and quality, as a dissertation for the degree of Doctor of Philosophy.

William Weltner
Professor of Chemistry

I certify that I have read this study and that in my opinion it conforms to acceptable standards of scholarly presentation and is fully adequate, in scope and quality, as a dissertation for the degree of Doctor of Philosophy.

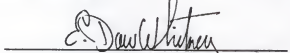

Ellsworth D. Whitney
Professor of Materials Science and Engineering

This dissertation was submitted to the Graduate Faculty of the Department of Chemistry in the College of Liberal Arts and Sciences and to the Graduate School and was accepted as partial fulfillment of the requirements for the degree of Doctor of Philosophy.

May 1998

Dean, Graduate School

LD
1780
1998
.B168